HHS Public Access

Author manuscript

Mol Neurobiol. Author manuscript; available in PMC 2021 March 01.

Published in final edited form as:

Mol Neurobiol. 2020 March ; 57(3): 1570–1593. doi:10.1007/s12035-019-01824-1.

Manganese acts upon Insulin/IGF receptors to phosphorylate AKT and increase glucose uptake in Huntington's Disease cells

Miles R. Bryan[1,2,3], **Kristen D. Nordham**[1,2,3], **Daniel I.R. Rose**[1,2,3], **Michael T. O'Brien**[1,2,3], **Piyush Joshi**[1,2,3], **Audra M. Foshage**[4], **Filipe M. Gonçalves**[7], **Rachana Nitin**[1,2,3], **Michael A. Uhouse**[1,2,3], **Michael Aschner**[7], **Aaron B. Bowman**[1,2,3,4,5,6,8]

[1]Dept. of Pediatrics, Vanderbilt University Medical Center, Nashville, TN

[2]Vanderbilt Brain Institute, Vanderbilt University Medical Center, Nashville, TN

[3]Dept. of Neurology and Biochemistry, Vanderbilt University Medical Center, Nashville, TN

[4]Department of Cell and Developmental Biology, Vanderbilt University Medical Center, Nashville, TN

[5]Vanderbilt Kennedy Center, Vanderbilt University Medical Center, Nashville, TN

[6]Vanderbilt Center for Stem Cell Biology, Nashville, TN,

[7]Albert Einstein College of Medicine, Bronx, NY,

[8]Purdue University, School of Health Sciences, West Lafayette, IN.

Abstract

Perturbations in insulin/IGF signaling and manganese (Mn^{2+}) uptake and signaling have been separately reported in Huntington's disease (HD) models. Insulin/IGF supplementation ameliorates HD phenotypes via upregulation of AKT, a known Mn^{2+}-responsive kinase. Limited evidence both in vivo and in purified biochemical systems suggest Mn^{2+} enhances insulin/IGF receptor (IR/IGFR), an upstream tyrosine kinase of AKT. Conversely, Mn^{2+} deficiency impairs insulin release and associated glucose tolerance in vivo. Here, we test the hypothesis that Mn^{2+}-dependent AKT signaling is predominantly mediated by direct Mn^{2+} activation of the insulin/IGF receptors, and HD-related impairments in insulin/IGF signaling are due to HD genotype-associated deficits in Mn^{2+} bioavailability. We examined the combined effects of IGF-1 and/or Mn^{2+} treatments on AKT signaling in multiple HD cellular models. Mn^{2+} treatment potentiates p-IGFR/IR-dependent AKT phosphorylation under physiological (1nM) or saturating (10nM)

Corresponding Author: Dr. Aaron Bowman, (bowma117@purdue.edu), (765)-494-2684.

Author contributions:

MRB and ABB designed all experiments. MRB performed most data analyses on all data. MRB, KN, DR, MO, RN, and MU carried out cell culture and experiments for all figures. PJ carried out hiPSC-derived cell culture and differentiations. AMF performed all qRT-PCR. FG performed all experiments and analysis in primary astrocytes. MA assisted in experimental design and interpretation. All authors read and approved the final manuscript.

Competing interests: The authors declare that they have no competing interests.

Data and material availability: The datasets during and/or analyzed during the current study will be made available using the Dryad data repository.

concentrations of IGF-1 directly at the level of intracellular activation of IGFR/IR. Using a multi-pharmacological approach, we find that >70–80% of Mn^{2+}-associated AKT signaling across rodent and human neuronal cell models is specifically dependent on IR/IGFR, versus other signaling pathways upstream of AKT activation. Mn^{2+}-induced p-IGFR and p-AKT were diminished in HD cell models, and, consistent with our hypothesis, were rescued by co-treatment of Mn^{2+} and IGF-1. Lastly, Mn^{2+}-induced IGF signaling can modulate HD-relevant biological processes, as the reduced glucose uptake in HD STHdh cells was partially reversed by Mn^{2+} supplementation. Our data demonstrate that Mn^{2+} supplementation increases peak IGFR/IR-induced p-AKT likely via direct effects on IGFR/IR, consistent with its role as a cofactor, and suggests reduced Mn^{2+} bioavailability contributes to impaired IGF signaling and glucose uptake in HD models.

Introduction

The essentiality of manganese (Mn^{2+}) is derived from its binding to and activation of several biologically indispensable enzymes, including Mn^{2+} superoxide dismutase, glutamine synthetase, pyruvate decarboxylase, protein phosphatase 2A (PP2A), and arginase (1). In addition, Mn^{2+} is a required cofactor for a variety of kinases, and can often compete with magnesium (Mg^{2+}) when at sufficiently high concentrations to activate others, including ATM and mTOR (2, 3). As the vast majority of kinases are either Mn^{2+}- or Mg^{2+}-dependent, Mn^{2+} can act as a potent cell signaling modifier. Mn^{2+} can activate ERK, AKT, mTOR, ATM, and JNK in vitro and in vivo (2, 4–13). As these kinases regulate transcription factors (CREB, p53, NF-kB, FOXO), Mn^{2+} can also modulate cell function at the transcriptional level (7, 14–16). Consequently, the roles of Mn^{2+} homeostasis and associated signaling in both the essentiality and toxicity of Mn^{2+} are an important area of investigation. However, it remains uncertain which Mn^{2+}-dependent enzymes are most sensitive to changes in Mn^{2+} homeostasis and the relationships between Mn^{2+}-biology and these signaling cascades.

In contrast, at high concentrations, Mn^{2+} can be neurotoxic, and this has been associated with risk for idiopathic parkinsonism and the Mn^{2+}-induced parkinsonian-like disease known as manganism (17–20). High environmental exposure to Mn^{2+} has been associated with specific occupational settings (welding, mining), exposure to industrial ferroalloy emissions, well water consumption in some regions, or parenteral nutrition (21–25). Of particular interest, Mn^{2+}-induced p-AKT has been observed in a variety of models and in Mn^{2+}-exposed patient populations (4, 10, 26–29). However, it is still unclear what the role of this response is or by which upstream signaling mechanism it occurs, though Mn^{2+}-induced p-AKT is not blocked by the antioxidant Trolox (30). Thus, the elucidation of the primary signaling mechanism behind Mn^{2+}-responsive AKT will be informative in the context of both basal Mn^{2+} homeostasis and Mn^{2+} neurotoxicity.

Insulin and IGF-1 are highly homologous growth factors which are necessary for a variety of peripheral processes, as well as essential for synaptic maintenance and activity, neurogenesis and neurite outgrowth, and neuronal mitochondrial function (31, 32). Insulin and IGF-1 bind to highly similar cell surface receptors which initiate an autophosphorylation cascade, independent of other kinases, which activates the insulin receptor (IR) and the IGF-1

receptor (IGFR). This causes subsequent activation of phosphatidylinositol-3-kinase (PI3K), insulin receptor substrates (IRSs), and other mediators activating the pro-growth AKT, mTOR, and ERK/MAPK pathways which have widespread roles in multiple biological processes. Dysregulation of these potent neurotrophic growth factors has been associated with neurodegenerative diseases, including HD, PD, and Alzheimer's disease (AD) (20, 33–49). However, while the vast majority of kinases in the human body are Mg^{2+} and/or Mn^{2+}-dependent, few studies have mechanistically elucidated how these metals maintain kinase signaling cascades in living biological systems or contribute to kinase-dependent pathology of neurodegenerative diseases.

Evidence supporting a role for insulin/IGF-1 synergistic cross talk with Mn^{2+} has been slowly amassing, but is incompletely understood. Mn^{2+} deficiency in rodent models reduces insulin production and causes glucose intolerance, while Mn^{2+} supplementation can protect against diet-induced diabetes rescue glucose intolerance, and increase insulin and IGF-1 ligand levels in rodents (50–59). Furthermore, Mn^{2+} administration stimulates insulin-linked glucose transport and related phosphodiesterase activity in adipocytes, though insulin/IGF receptor activity was not investigated (60). Two prior studies have examined how supra-physiological Mn^{2+} (1–10mM) activates insulin receptor activity using non-living, permeabilized rat adipocytes or purified biochemical systems and have shown that Mn^{2+} directly increases net autophosphorylation of IR/IGFR by both enhancing kinase activity and inhibiting receptor dephosphorylation (61, 62). Further, the peak/maximum *in vitro* kinase activity of IR/IGFR is higher in the presence of Mn^{2+}, than with Mg^{2+}. Finally, a previous study reported that JB1, an IGFR1 antagonist, can block Mn^{2+}-induced IGFR-AKT-mTOR phosphorylation in the preoptic area of prepubertal rats (10). Together, these data provide a strong premise to examine this signaling pathway at a cellular level and suggest Mn^{2+} may be a critical mediator of insulin/IGF-1 homeostasis and downstream signaling, including AKT (27–29, 52, 56–58, 63). However, the understanding of Mn^{2+}-IGF synergy lacks mechanistic insight of the direct site-of-action of Mn^{2+} on IGFR/IR-AKT signaling and requires confirmation of this mechanism in living systems under biologically-relevant, sub-cytotoxic concentrations of Mn^{2+} (1–500μM). Furthermore, elucidation of an initial site-of-action for Mn^{2+} may bridge the mechanistic gap between non-living and in vivo systems—directly connecting the role of Mn^{2+}-induced receptor kinase activity to the changes seen in Mn^{2+}-responsive metabolism in vivo, such as glucose tolerance.

HD is an autosomal dominant, neurodegenerative disease caused by an expanded CAG repeat within exon 1 of the Huntingtin (HTT) gene. Through a yet unknown pathogenesis, this expanded trinucleotide causes specific cell death in the medium spiny neurons of the striatum, leading to a variety of symptoms—most notably chorea. This disease has variable progression, but is ultimately fatal. There is no cure for HD, but drugs can target symptoms with variable efficacy. Recent research has shown that IGF-1 treatment in HD models results in robust amelioration of a wide-array of phenotypes via AKT signaling-mediated mechanisms. The results of this treatment include: an increase in autophagic function and mutant HTT (mutHTT) aggregate clearance; restoration of mitochondrial function; regularization of energy metabolites; HTT serine 421 phosphorylation; and medium spiny neuron health. Perhaps most importantly, IGF treatment can rescue motor abnormalities and early mortality in HD mouse models (32, 64–68). Furthermore, although HD is primarily a

neurological disease, HD patients develop type 2 diabetes mellitus at a higher incidence than healthy controls and diabetic phenotypes can be rescued via IGF-1 treatment in HD models (32, 69–71). These data warrant further investigation into 1) the factors which contribute to dysregulated IGF-AKT signaling in HD and 2) the mechanism through which IGF-1 effectively treats some HD phenotypes.

Here, we assessed whether the synergistic effects of Mn^{2+}+IGF occur via the ability of Mn^{2+} to directly act on IR/IGFR to elicit downstream AKT phosphorylation and determined if this mechanism is disrupted in a disease model system (HD) associated with a Mn^{2+} *deficiency*. While few human studies have examined Mn^{2+} levels in post-mortem HD brains, existing studies have found either no change in striatal Mn^{2+} or reductions only in the cortex (72–74). Prior studies in our lab have reported reduced Mn^{2+} uptake in in vitro HD cell models and the striatum of the YAC128 HD mouse model—indicative of a defect in Mn^{2+} accumulation (75–77). We have shown that Mn^{2+} treatment rescues deficient arginase activity in HD mice (78) and that in HD cell lines, this reduced Mn^{2+} uptake manifests as reduced Mn^{2+}-induced activation of ATM-p53 and AKT cell signaling (14, 79). In contrast, changes in cholesterol metabolism appear unaffected by Mn^{2+} (80). Recently, we have established that Mn^{2+} induced p-AKT is dependent on PI3K, a downstream mediator of IR/IGFR, in STHdh cells (28). As AKT signaling mediates the restorative effects of IGF-1 administration in HD mouse models, we hypothesize here that Mn^{2+} promotes AKT signaling through an upstream IGFR-1-dependent mechanism, and that reduced Mn^{2+} uptake should manifest as impaired Mn^{2+}→ IR/IGFR→ PI3K→ AKT signaling and contribute to well-established IGF-related deficits in HD. This study aimed to 1) define the synergistic co-regulation between Mn^{2+} and IGF on AKT signaling in various cellular models, 2) determine the initial, mechanistic target of Mn^{2+}, which allows for downstream AKT activation, 3) elucidate the effects of Mn^{2+}+IGF co-treatment on impaired IGFR/IR-AKT signaling in HD cells, and 4) investigate the effects of Mn^{2+} on glucose uptake, a downstream process of AKT signaling which is perturbed in HD patients and mouse models. These findings provide proof-of-principle evidence that Mn^{2+} supplementation could improve efficacy of IGF-centric therapies in HD.

RESULTS

Mn^{2+} and IGF exhibit synergistic regulation of p-AKT expression which is diminished in HD cells

Previous studies suggest that Mn^{2+} acts as an insulin mimetic, and also increases the kinase activity at the insulin receptor itself; however, these findings were primarily established using recombinant enzymes or permeabilized cellular models (61, 62). Furthermore, Mn^{2+} has been shown to activate insulin/IGF-responsive kinases and signaling pathways, including AKT. Given these observations, we hypothesized that Mn^{2+} potentiates IGF-induced p-AKT expression in neuronal cells. We examined p-AKT (Ser^{473}) expression after 1hr serum deprivation in HBSS, followed by 3hr treatment with Mn^{2+}/IGF in HBSS. For these experiments, we treated STHdh cells with 1nM IGF, which has been reported to be near physiological concentration (81). Normal human brain Mn^{2+} concentrations are estimated to be ~20–55μM (82). Mn^{2+} begins to induce in vitro cytotoxicity after 24hr, 100–200μM

Mn^{2+} exposures, depending on cell type (14, 79). Across short exposures (3hrs), we did not observe any decrease in cell viability following 500μM Mn^{2+} in any cell type (Supplemental Figure 7A, B). Thus, for our experiments, we utilize sub-cytotoxic 50–500μM Mn^{2+} exposures based on cell type and exposure duration. Mn^{2+}/IGF co-exposure induced a nearly 30-fold increase in p-AKT, ~15 times higher than 500μM Mn^{2+} alone, and ~3 times higher than IGF alone (Fig 1A). This confirms a synergistic regulation of AKT signaling by Mn^{2+} and IGF in living cells. Furthermore, treatment with Mn^{2+} alone resulted in an insignificant increase in p-AKT, suggesting that Mn^{2+}-induced p-AKT is dependent on the presence of an upstream ligand, such as IGF or insulin. To examine this further, we treated WT Q7/Q7 STHdh cells with 50 or 500μM Mn^{2+} in normal serum-containing media or in serum-free HBSS following 1hr serum deprivation. Consistent with previous results, 3hr treatment with Mn^{2+} (50 or 500μM) did not cause a significant increase in p-AKT in serum-free HBSS (though 500μM trended towards increase p-AKT in HBSS), but did significantly increase p-AKT in serum-containing media at both concentrations. *This suggested that a potential interaction with a serum component, such as insulin or IGF, is essential for Mn^{2+}-induced p-AKT* (Fig 1B).

The STHdh Q111/Q111 HD cell model exhibits both a basal Mn^{2+} uptake deficit as well as a reduced net Mn^{2+} accumulation after an exogenous exposure, making it an ideal model to study Mn^{2+}-induced IGF signaling and the consequences of perturbations to this system (14, 79). Thus, we hypothesized that this cell model would also exhibit reduced Mn^{2+}/IGF-induced p-AKT expression. This would be consistent with other studies demonstrating defects in AKT signaling in HD (65, 66, 83–85). Indeed, the Q111 HD cell model exhibited reduced Mn^{2+}/IGF-induced p-AKT expression following a 3hr Mn^{2+} exposure in serum-free media (Fig 1C). However, treatment with IGF+500μM Mn^{2+} in the Q111 HD cells restored p-AKT expression to levels seen with IGF+200μM Mn^{2+} in the Q7 WT model. Total AKT levels were unchanged by Mn^{2+} after 3hrs in media or HBSS (Supp Fig 1A). *This confirms reduced Mn^{2+}-induced p-AKT in this HD cell model, and demonstrates that the Mn^{2+}-uptake defect can be attenuated via higher doses of Mn^{2+} treatment, compensating for the uptake deficit.*

We reasoned that if Mn^{2+} acts as an insulin/IGF “mimetic” by increasing ligand concentration or ligand-receptor occupancy, Mn^{2+} should be unable to further activate p-AKT in the presence of saturating concentrations of insulin/IGF. We determined that the saturating concentration of IGF-1 in serum-containing media for p-AKT after 24hrs is approximately 10nM (Supp Fig 1B). Co-treatment with 10 nM IGF-1 and 50 μM Mn^{2+} for 24hrs in normal (serum-containing) media resulted in supra-additive p-AKT responses (>2fold compared to IGF or Mn^{2+} alone) in STHdh and p-AKT and p-S6 in uninduced, differentiated PC12 cells mirroring the effects seen in the 3hr exposures above (Fig 1D–F, Supp Fig 1C). P-p53, another Mn^{2+}-responsive pathway in these cells, was indistinguishable between Mn^{2+} and Mn^{2+}+IGF exposed conditions, demonstrating that this is not a broad effect across all Mn^{2+}-responsive pathways (data not shown). As expected, Mn^{2+}-induced p-AKT was blunted in HD cells following 24hr exposure. Furthermore, Mn^{2+}/IGF co-treatment significantly increased p-AKT activation compared to the effects of Mn^{2+} or IGF alone in the Q111 HD cells (Fig 1D), similar to Fig 1C. Total AKT levels (Pan-AKT) were not significantly different in any of the conditions and p-AKT (Thr^{308}) showed a highly

similar trend to Ser^{473}; thus, going forward, we only quantified p-AKT (Ser^{473}) (Supp Fig. 1D). *Together, these data suggest that Mn^{2+} synergistically increases the maximal activity of the AKT pathway, even under saturating concentrations of ligand, but expression of mutHTT dampens this effect.*

Phosphorylation of AKT is specific to Mn^{2+} and not shared by other cation exposures at sub-cytotoxic concentrations

We hypothesized that Mn^{2+}-induced p-AKT is a consequence of a Mn^{2+}-responsive kinase upstream of AKT rather than a broad effect of heavy metal exposure, such as reactive oxygen species (ROS) accumulation. In other words, if Mn^{2+} is acting as a cofactor for an upstream kinase, then its activity on downstream proteins should be unique to Mn^{2+} vs other metal cations not capable of serving as kinase cofactors. Thus, we determined 1) whether other metal cations are capable of increasing p-AKT similarly to Mn^{2+} and 2) if HD genotype cells exhibit reduced p-AKT in response to other metal cations. We tested a battery of cations (Fe^{3+}, Cu^{2+}, Mg^{2+}, Zn^{2+}, Cd^{2+}, Ni^{2+}, and Co^{2+}) and examined p-AKT expression after 24hrs. For these experiments, we used concentrations which are near the toxic threshold in these cells after 24hr exposures as shown in our previous work (79) and found that Mn^{2+} was the only cation which elicited a significant p-AKT response, and thus, the only metal which exhibited an HD phenotype. Cu trended towards an increase in p-AKT but this was not significant (Fig 2A–C). Although other cations were unable to significantly increase p-AKT under these sub-cytotoxic concentrations, we hypothesize that higher concentrations of some cations may also increase p-AKT via a cytotoxic response. As Mn^{2+} and Mg^{2+} often act as cofactors with the same enzymes, we supplemented the media for these cells with an additional 50μM Mg^{2+} or Mn^{2+} (though DMEM contains high physiological concentrations of Mg^{2+}) increasing the available combined pool of Mg^{2+}/Mn^{2+}, and did not observe Mg^{2+}-induced p-AKT (Fig 2C). Consistent with our results in living cells, these studies observed that the combination of Mn^{2+}+Mg^{2+} evoked higher insulin receptor activity (61, 62). *This supports the hypothesis where the role of Mn^{2+} to increase p-AKT expression is metal ion-specific, and furthermore, that Mn^{2+} is able to do this under saturating concentrations of Mg^{2+} (a known, competing cofactor for many kinases).*

Reduced Mn^{2+}-induced p-AKT in HD cells persists under prolonged physiologically-relevant Mn^{2+} exposures

While we observed reduced Mn^{2+}-induced p-AKT in HD cells after high dose, acute Mn^{2+} exposure, we wanted to assess whether this phenotype would persist under lower dose, subacute, week-long exposures. Thus, we treated STHdh cells for 1 week with 1, 5, or 10 μM Mn^{2+}. In Q7/Q7 cells, Mn^{2+}-induced p-AKT was observed after a 7-day exposure, with 5 and 10 μM eliciting the highest effect (Fig 2D, E). *Phosphorylation of AKT was almost completely unresponsive in Q111/Q111 HD cells to low-dose Mn^{2+} exposure, confirming that the HD genotype perturbation persisted under these subacute treatments. Additionally, this suggests Mn^{2+}-induced p-AKT occurs with changes in Mn^{2+} homeostasis well below the toxic threshold.*

Normalization of net Mn^{2+} uptake ameliorates Mn^{2+}-induced p-AKT defect in HD cells

The Q111/Q111 HD STHdh cells exhibit reduced Mn^{2+}-induced p-AKT across several treatment paradigms (Fig 1C–D, 2D–E). If reduced Mn^{2+}-induced p-AKT in HD cells is dependent on intracellular Mn^{2+} levels, normalization of intracellular Mn^{2+} uptake in the HD cells to match WT levels would be predicted to ameliorate Mn^{2+}-induced p-AKT differences between the genotypes. KB-R7943 is a drug which inhibits the sodium-calcium uniporter (NCX1/3) and normalizes Mn^{2+} uptake in these HD cells by an unknown mechanism. This drug was previously used to normalize Mn^{2+} uptake and Mn^{2+}-induced p-p53, concurrently(86). We confirmed this result and observed significant increases in Mn uptake in HD cells when treated with Mn and KB-R7943 (Supplemental Fig 2A). When HD cells were exposed to KB-R7943 and 50 μM Mn^{2+}, Mn^{2+}-induced p-AKT was restored to levels observed in WT cells treated with Mn^{2+} alone (Fig 2F, G). *This suggests reduced Mn^{2+}-induced cell signaling levels are driven by the decreased intracellular Mn^{2+} in this model. Although the mechanism by which KB-R7943 restores Mn^{2+} uptake is unknown, these data also demonstrate that the drug can increase the bioavailable pool of Mn^{2+}, as opposed to merely sequestering Mn^{2+} in metabolically inaccessible regions of the cell.*

Expression of mutHTT is sufficient to reduce Mn^{2+}-induced p-AKT in differentiated PC12 cells

Next, we sought to confirm if other HD model cells lines exhibit reduced Mn^{2+}-induced p-AKT. First, we utilized differentiated PC12 cells which express WT HTT but are capable of additional ponasterone A-induced HTT expression (23, 74, 145 CAG or CAA). These cells were differentiated into a neuronal phenotype by treatment with nerve growth factor (NGF) over the course of a week and expressed tyrosine hydroxylase, indicating a catecholaminergic population (data not shown). After 7 days of differentiation with NGF and mutHTT induction with ponasterone A, 145 CAG-expressing PC12 cells exhibited reduced Mn^{2+}-induced p-AKT compared to uninduced counterparts (Fig 3A,B). Induction of 74CAG mutHTT resulted in a modest, but insignificant, reduction in Mn^{2+}-induced p-AKT, and, as expected, induction of 23 CAG HTT had no effect. (data not shown). Pan AKT and pan S6 were unaffected in all conditions, similar to STHdh cells (Fig 3A, Supp Fig 1C). Mn^{2+} induced p-S6 was unaffected by mutHTT expression (data not shown). *Together, these data demonstrate impairments in Mn^{2+} homeostasis and signaling are present in a variety of HD cell lines and occur within days of mutHTT expression.*

Mn^{2+} potentiates IGF-induced p-IR/IGFR expression which is blunted in HD cells

We established a specific, synergistic effect on p-AKT signaling by Mn^{2+}/IGF co-treatment which was diminished in several HD cell lines. We sought to elucidate the mechanistic target of Mn^{2+} which allows for the synergistic effect on p-AKT. This target is likely responsible for driving the reduced Mn^{2+}-induced p-AKT in HD models. As Mn^{2+} is a known cofactor for a variety of kinases, including IR/IGFR(61, 62), we hypothesized that Mn^{2+} may be directly interacting with IR/IGFR to induce p-AKT. To our knowledge, phospho-specific antibodies do not exist which distinguish between p-IR or p-IGFR, as they are phosphorylated at highly similar residues (87, 88). Thus, to examine this, we co-treated Q7 WT and Q111 HD STHdh cells with Mn^{2+}/IGF for 3hrs following a 1hr serum deprivation

and assessed p-IR/IGFR levels. We found that Mn^{2+} potentiated IGF-induced IR/IGFR phosphorylation. Further, Mn^{2+}-induced p-IR/IGFR levels were blunted in HD cells but co-treatment with IGF+500μM in HD cells elicited similar p-IR/IGFR expression as IGF +200μM Mn^{2+} in WT cells (Fig 4A,B). These observations mirror the effects of Mn^{2+} on p-AKT expression in Fig 1C. *Altogether, these data support a role for Mn^{2+} directly increasing IR/IGFR activity, thereby activating downstream signaling including AKT*.

Mn^{2+} reduces total IGFR protein expression and IGFR mRNA expression

Our data suggest that Mn^{2+} can increase maximal IGF-induced p-AKT activity. Thus, we wanted to assess whether this leads to negative feedback on total IGFR expression. We hypothesized that Mn^{2+} (in conjunction with IGF) exposure *reduces* total IGFR expression after 24hrs to reduce overall activity of the AKT pathway. Indeed, 50μM Mn^{2+} treatment, similarly to IGF treatment, decreased total IGFR expression by ~50%—perhaps acting through a negative feedback mechanism to prevent overactivation of the pathway (Fig 4C,D). Unlike IGFR, Mn^{2+} did not reduce total IR expression in WT or HD cells, but IGF treatment alone decreased total IR expression specifically in HD cells (Fig 4E,F). Mn^{2+} exposure for only 3hrs in media or HBSS left total IGFR unchanged (Supp Fig 1A).

To determine whether the Mn^{2+}-induced reduction in total IR/IGFR expression is mediated, at least in part, by a transcriptional mechanism, we assessed the effects of Mn^{2+} on IR/IGFR mRNA expression. We found that 24hr Mn^{2+} (or Mn^{2+}+IGF) treatment reduced IGFR mRNA expression and Mn^{2+}+IGF co-treatment modestly reduced expression of IR mRNA expression in both genotypes, suggesting that Mn^{2+} may have a more specific effect on IGFR signaling than that of IR (Fig 4G,H). Mn^{2+} specifically reduced IR mRNA expression in HD cells only. The HD genotype did not affect basal IGFR or IR mRNA expression. Additionally, we assessed mRNA expression of IRS2, a downstream partner in insulin/IGF signaling. IRS2 mRNA was greatly reduced in HD cells and Mn^{2+} exposure reduced IRS2 mRNA in Q7 cells only (Fig 4I). *Together these data demonstrate that Mn^{2+} also modulates total IR/IGFR protein expression via transcriptional downregulation*.

Mn^{2+}-induced p-AKT is completely abrogated by pharmacological IR/IGFR inhibition

After observing that Mn^{2+} and IGF exert synergistic effects on p-AKT and p-IR/IGFR, we hypothesized that IGF and Mn^{2+} may be cooperatively activating on the same upstream kinase to increase AKT phosphorylation. Previously, we found that Mn^{2+}-induced p-AKT is dependent on PI3K in these cells, as LY294002, a PI3K inhibitor, can completely abrogate Mn^{2+}-induced p-AKT (28). This narrows down the possible targets to upstream activators of PI3K including IR/IGFR. Given these data and the prior evidence of a role for IR/IGFR signaling, we hypothesized some or all of Mn^{2+}-induced p-AKT is IR/IGFR-dependent. IR/IGFR are essential to neuronal differentiation, development, and homeostasis which complicates the generation and use of knockout cell lines, and less-than-complete efficiency of siRNAs would allow for remaining receptors to compensate (31, 32). Thus, we turned to pharmacological modulation of IR/IGFR. While small molecules allow dosing to achieve near-complete inhibition, they are prone to off-target effects. Thus, to increase the rigor of our findings we employed a battery of four ATP-competitive IR/IGFR inhibitors (BMS-536924, BMS-754807, Linsitinib (OSI-906), and NVP-AEW541) so that multiple

inhibitors could be used across each cell line. Additionally, these inhibitors have different known off-target proteins (Fig 5A), so any shared effects by the inhibitors are likely via IR/IGFR only (89–92).

Using these various inhibitors across STHdh and PC12 cells, we found 1) Mn^{2+}-induced p-AKT was inhibited in STHdh cells with 100nM BMS-536924 (Fig 5B, C), 0.1–1μM Linsitinib (Fig 5D,E), or 0.1–1μM NVP-AEW541 (Fig 5D,F) and 2) Mn^{2+}-induced p-AKT and p-S6 was blocked with 100nM BMS-536924 in PC12 cells (Fig 5G–H, Supp Fig 1C). In PC12 cells, >100% of Mn^{2+}-induced p-AKT (below vehicle levels) and 59% of Mn^{2+}-induced p-S6 was inhibited using 100nM BMS-536924 (near the estimated IC50 concentration) (Fig 5G–H, Supp Fig 6B). BMS-536924 inhibited 46% of Mn^{2+}-induced p-AKT at this approximate IC50 in STHdh cells (Fig 5B, C, Supp Fig 6A). 100nM linsitinib (approximately the IC50 for IR, 3X IC50 for IGFR) inhibited 71% of Mn^{2+}-induced p-AKT (Fig 5D, E, Supp Fig 6A). 100nM NVP-AEW541 (approximately 65–70% the IC50 for IR and IGFR) inhibited 54% of Mn^{2+}-induced p-AKT (Fig 5D, F, Supp Fig 6A). At 1μM (10-fold higher), Linsitinib and NVP-AEW541 inhibited 81% and 65% of Mn^{2+}-induced p-AKT. Additionally, Linsitinib, the most specific of the inhibitors, was able to inhibit 60% of Mn^{2+}+IGF induced p-AKT in STHdh cells at 100nM (Fig 5D, E, Supp Fig 6A). We confirmed that these inhibitors blocked IGF-induced p-IR/IGFR in the STHdh cells (data not shown). *The high degree of dose-dependent inhibition by multiple IGFR inhibitors suggests that the vast majority of Mn^{2+}-induced IGFR/AKT signaling is IR/IGFR-dependent*. IR/IGFR exhibit autophosphorylation upon binding to insulin/IGF (and necessary co-factors) and do not require the kinase activity of other upstream kinases for activation. *With this in mind, this data in addition to our observed Mn^{2+}-induced p-IGFR/IR* (Fig 4A) *also suggest Mn^{2+} is activating directly at the level of the IR/IGFR (or affecting extracellular insulin/IGF production or binding) as opposed to another kinase upstream of these tyrosine kinase receptors*

Non-neuronal cell types also exhibit IR/IGFR-dependent, Mn^{2+}-induced p-IGFR/p-AKT

We hypothesized Mn^{2+}-induced p-AKT was not specific to NPCs and would be present in other cell types. To investigate this, we exposed isolated primary rat astrocytes to 500μM Mn^{2+}, 1nM IGF, or both for 3hrs following a 1hr serum deprivation. As in neuroprogenitors, addition of Mn^{2+}+IGF increased p-AKT significantly more than either Mn^{2+} or IGF alone (Fig 6A, B). Additionally, we tested whether Mn^{2+}-potentiated p-IGFR/p-AKT occurred in other non-neuronal, peripheral cell types—immortalized 3T3 fibroblasts and HEK293 kidney cells. Similar to what we observed in STHdh cells, a 3hr 500μM Mn^{2+} exposure did not activate p-IGFR, p-AKT, or p-S6 in the absence of IGF-1 in these cells (Fig 6C–E, Supp Fig 2B). This confirms that Mn^{2+}-induced IGFR/AKT signaling requires the presence of ligand (IGF-1 or insulin) across a variety of cell types. In NIH3T3 and HEK293 fibroblasts, Mn^{2+}+IGF increased p-AKT and p-IGFR expression more than IGF or Mn^{2+} alone after 1hr serum deprivation (Fig 6C, E, Supp Fig 2B). This corroborates the finding that the synergistic effects between Mn^{2+} and IGF are not restricted to neuronal cells. Additionally, Linsitinib (1μM) completely inhibited p-IGFR/IR (>98%) in 3T3 cells and the vast majority of Mn^{2+}+IGF-induced p-AKT (≥80%) could also be blocked by Linsitinib or LY294002 (PI3K inhibitor). In HEK293 cells, the vast majority of p-IGFR (≥98%) was inhibited with

Linsitinib, but only 40% of Mn^{2+}-induced p-AKT was blocked, suggesting Mn^{2+}-induced p-AKT is less dependent on IGFR/IR in HEK293 cells than in 3T3 cells. (Fig 6F,H, Supp Fig 6B). Furthermore, by comparing the degree of p-IGFR/IR inhibition to p-AKT inhibition by Linsitinib, we can estimate the percentage of Mn^{2+}-induced p-AKT which is dependent on p-IGFR/IR [(% of p-AKT inhibition) / (% of p-IGFR/IR inhibition)]. Using this calculation, we estimate that 99% of Mn^{2+}-induced p-AKT in 3T3 cells and 41% in HEK293 cells is dependent on p-IGFR (Supp Fig 6B). This confirms that Mn^{2+}-induced p-AKT is IR/IGFR-dependent in these non-neuronal cell types as well, particularly 3T3 cells. P-S6 also trended with p-AKT across conditions in 3T3 cells, but due to the variability in Mn^{2+}+IGF treatment, this trend was not significant (Fig 6D,G). Additionally, we found that there was only a 62% correlation between p-S6:p-IGFR/IR inhibition in 3T3 cells and 19% correlation in HEK293 cells, suggesting Mn^{2+}-induced p-S6 is much less dependent on IGFR/IR than p-AKT (Supp Fig 6B). *These data provide strong evidence that Mn^{2+}-induced p-IGFR and p-AKT are not restricted to specific neuronal lineages*.

Mn^{2+}-induced IGF signaling is dampened in human induced pluripotent stem cells (hiPSC)-derived striatal neuroprogenitors and is blocked by IGFR inhibition

We wanted test whether the HD-dependent IGF signaling defect observed in cell line models of HD would also be seen in a non-transformed human neuronal model. We chose to utilize the hiPSC-derived Islet-1-expressing striatal neuroprogenitor cells (NPCs) which are derived via a protocol designed in our lab (14). After a 24hr exposure, Mn^{2+}-induced p-AKT in Islet-1+ hiPSC-derived striatal-like NPCs from HD patients was not significantly different than control cells; also, p-IGFR and p-S6 (often used as a readout for mTOR activity) were both induced by Mn^{2+}, but neither was differentially affected in HD cells (data not shown). However, in striatal NPCs, we observed that under these conditions, IGF-1 was unable to activate p-AKT, likely because their normal NPC media conditions contain saturating insulin (Supp Fig 3). Thus, this standard striatal NPC media conditions are not a biologically-relevant setting to study IGF signaling or disease-relevant IGF/AKT-centric phenotypes. However, the data do suggest that Mn^{2+} can upregulate maximal AKT phosphorylation even under insulin-saturating concentrations.

To circumvent this issue of saturating insulin in the media, we found that growth factor/insulin deprivation prior to exposure allowed detection of p-IGFR in these NPCs and decreased variability in downstream p-AKT/p-S6 signaling. Thus, we used a 3hr growth factor deprivation followed by 3hr exposure with Mn^{2+} and/or IGF, and then assessed p-AKT, p-S6, and p-IGFR expression. Cells were treated under insulin/IGF-deprived conditions (though there are likely trace amounts of insulin/IGF left behind or produced by the cells themselves) and in the presence of 1 nM IGF. IGF, as expected, stimulated p-IGFR and p-AKT expression, though there were no apparent differences in magnitude between control and HD patient cells. Surprisingly, IGF did not significantly increase p-S6 expression in control or HD cells (Supp Fig 5A, B).

A 200–500μM Mn^{2+} treatment for 3hrs increased p-AKT and 500μM treatment increased p-IGFR and p-S6 in control cells (Fig 7A–C, Supp Fig 4). p-AKT and p-IGFR responses to Mn^{2+} were greater in conditions with IGF, suggesting a synergistic relationship similar to

the one observed in STHdh cells (Fig 7A,B, Supp Fig 4). Mn^{2+} was able to significantly increase p-IGFR, p-AKT, and p-S6 in the absence of added IGF (Fig 7A–C, Supp Fig 4). This may be a result of trace IGF left behind in the media or generation of IGF by the cells themselves. In HD cells, Mn^{2+} induced p-AKT was only significant after 500μM Mn^{2+} treatment, and neither p-IGFR or p-S6 were significantly impacted (Fig 7A, B, Supp Fig 4). Mn^{2+}-induced p-S6 is completely diminished without the addition of IGF-1 to HD cells (Fig 7C, Supp Fig 4). We found that total levels of IGFR, AKT, and S6 did not change with Mn^{2+} or IGF exposures, and thus we only quantified p-IGFR, p-AKT, and p-S6 (Supp Fig 4C–F). *These results confirm that Mn^{2+}-induced IGF signaling is diminished in HD patient-derived striatal-like NPCs*.

We then assessed whether BMS-536924 and/or BMS-754807 could block Mn^{2+}-induced IGF signaling in these cells, to validate that IR/IGFR signaling was required for the effects on p-IGFR, p-AKT and/or p-S6 effects. Similar to other cells tested, with some trending exceptions, both inhibitors blocked a portion of Mn^{2+}-induced p-IGFR, p-AKT, and p-S6 in both control (Fig 8A,B) and HD (Fig 8C,D) cells at ~IC50 concentrations (100nM for BMS-536924 and 2nM for BMS-754807). In HD cells, we detected significant inhibition on Mn-induced p-IGFR and p-S6 as drug application often decreased expression below vehicle levels. 100nM BMS-536924 inhibited 48% of Mn^{2+}-induced p-AKT, but at higher concentrations (1μM) could inhibit Mn^{2+}-induced p-AKT even further, achieving >71% inhibition (Fig 8A). BMS-754807 inhibited 57% of Mn^{2+}-induced p-AKT at its ~IC50 concentration (100nM) (Fig 8B). We estimate ≥68% of Mn^{2+}-induced p-AKT is dependent on p-IGFR/IR across both inhibitors (74–80% with BMS-536924, 68% with BMS-754807) in Mn^{2+}+IGF treated control cells. These inhibitors were less effective at inhibiting Mn^{2+}-induced p-S6, similar to 3T3 and HEK293 cells (Supp Fig 6C). These two inhibitors also inhibited basal p-IGFR, p-AKT, and p-S6 (Supp Fig 5C,D). *Together, these results suggest that, similar to STHdh andPC12 cells, in human derived NPCs: 1) Mn^{2+}-induced IGF signaling is dampened in HD cells, and 2) Mn^{2+}-induced p-AKT is dependent on IR/IGFR*.

Mn^{2+} promotes IGF receptor phosphorylation via intracellular interactions

Since the vast majority of Mn^{2+}-induced p-AKT was dependent on IR/IGFR (Fig 5, 8) which autophosphorylate and do not require the presence of upstream kinases, our data suggest that Mn^{2+} is either 1) directly impinging on IGFR/IR activity intracellularly (kinase domain) or 2) affecting insulin/IGFR production or receptor binding, extracellularly. To test this, we exposed hiPSC-derived NPCs to Mn^{2+} for 3hrs, followed by a thorough set of media washes. After washing off the exogenous Mn^{2+}, we added Mn^{2+}-free HBSS with or without 1nM IGF-1 to the cells. We reasoned that if Mn^{2+} activates IGFR/AKT extracellularly, pre-exposure with Mn^{2+} should not potentiate IGF-induced IGFR/AKT/S6 phosphorylation, as extracellular Mn^{2+} would be negligible in the presence of IGF. However, if Mn^{2+} acts intracellularly to promote IGFR activity, pre-exposure with Mn^{2+} will lead to a lasting increase of intracellular Mn^{2+} and should still cause additive increases to IGF-1-induced signaling. Consistent with an intracellular action of Mn^{2+}, we found that pre-exposure with Mn^{2+} was able to increase p-IGFR and p-AKT expression (Fig 9A–C). Similar to WT cells in Fig 7C, Mn^{2+} only increased p-S6 in conditions when IGF was absent (Fig 9D), suggesting the synergy between Mn^{2+}+IGF co-treatment on p-S6 signaling may be quite

different from that of p-AKT and p-IGFR in these cells. *Together, these data support our hypothesis that Mn^{2+} acts on IGFR via intracellular interactions*.

Acute Mn^{2+} exposure increases glucose uptake in HD cells only

To determine whether Mn^{2+}-associated IGF/AKT signaling is associated with the decreased IR/IGFR-related functional processes in HD cells, we examined glucose uptake. IGF/AKT signaling has been associated with energy and glucose homeostasis, both of which are perturbed in HD and even precede onset of primary symptoms in HD mice (93–99). Accordingly, we observed that HD STHdh cells exhibit ~60% reduction in glucose uptake compared WT, consistent with published reports in HD patients (100). We then measured glucose uptake in STHdh cells after a 24hr Mn^{2+} exposure. Consistent with an insulin-mimetic role of Mn^{2+}, 100 μM Mn^{2+} was able to modestly, but significantly, increase glucose uptake in HD cells, but not WT cells—although glucose levels in HD cells did not reach WT levels (Fig 10A). We did not observe any effect at 50 μM (data not shown). This increase in glucose uptake was highly consistent with significant increases in p-AKT in HD cells-occurring only at 75 or 100uM (p-p53 was also used as a positive control for Mn-induced signaling on the representative blot, but not quantified) (Fig 10B, C). 100uM Mn treatment in HD cells increased Mn^{2+} uptake to levels equal in magnitude to WT cells treated with 50uM Mn^{2+}, although there were still significant differences in Mn uptake between genotypes at 50uM, 75uM, and 100uM (Supplemental Figure 7H). *This HD-specific effect provides evidence that homeostatic Mn^{2+} levels play a role in maintaining glucose homeostasis, and suggests that reductions in bioavailable Mn^{2+} (such is the case is with Q111/Q111 cells) contribute to perturbations in glucose uptake, a known phenotype in HD patients*.

Discussion

Several laboratories have observed Mn^{2+}-induced insulin/IGF-related signaling (primarily AKT) in cell and rodent models, but the direct mechanism by which Mn^{2+} stimulates these pathways was unclear (10, 27–29). Here, we sought to define the ambiguous relationship between Mn^{2+} and insulin/IGF signaling, and how this interaction mediates Mn^{2+}-induced signaling—namely AKT. We also wanted to investigate how perturbations in this relationship may manifest in HD—as models of HD exhibit reduced Mn^{2+} uptake and defective insulin/IGF signaling.

Here, we observed that IGF and Mn^{2+} work synergistically to regulate insulin/IGF activity. In the presence of IGF, Mn^{2+} was able to increase peak AKT signaling more than near-physiological (1nM) or saturating (10nM) concentrations of IGF alone (Fig 1C, D) (101). Since Mn increased p-AKT more than saturating concentrations of IGF alone, this suggest Mn can increase maximal IGF-dependent activation of p-AKT in living cells. Furthermore, Mn^{2+} was able to increase phosphorylation of IR/IGFR, in the presence of physiological levels of IGF (1nM) (Fig 4A, 6, 7B). Additionally, after 24hr exposure, Mn^{2+} decreased total IGFR protein expression and IGFR mRNA expression (Fig 4C–E). We hypothesize that sustained exposure with Mn^{2+} causes a negative feedback loop to reduce total IGFR protein by decreasing IGFR mRNA, thus dampening total IGF signaling activity, though we have no

explicitly tested this mechanistically. These findings are consistent with a previous study showing that Mn^{2+} inhibits insulin receptor dephosphorylation, in addition to increasing kinase activity (61). This sustained activity would likely require a negative feedback loop to prevent continuous stimulation of the pathway, facilitating restoration of homeostasis. However, presently, it is unclear why Mn-induced decreases in IGFR mRNA and protein are similar between WT and HD cells although intracellular Mn and Mn-induced p-IGFR/AKT are significantly different. This might suggest that these decreases in total protein and mRNA may actually be independent of intracellular Mn and subsequent kinase signaling, or that Mn levels are differentially affected in cytoplasmic and nuclear cellular compartments. Future studies should pharmacologically or genetically investigate this mechanism further and will likely need to measure mRNA transcription, stability, and translation. Together, our data demonstrate that Mn^{2+} is able to modulate insulin/IGF signaling via multiple avenues directly related to the IR and IGFR, and thereby impacts downstream p-AKT levels. Furthermore, it is possible that cellular Mn^{2+} levels could be further regulating this signaling via means which we have not examined in this study, such as receptor internalization, Mn^{2+}-induced phosphatase activity, or interactions with autophagy or the proteasome. Thus, to fully understand the complete coordination between Mn^{2+} homeostasis and IGF signaling, all of these distinct modalities of IGF signaling regulation (transcription, mRNA stability, and translation) must be assessed in the future.

Mn^{2+}-induced AKT signaling was first reported years ago, specifically in the context of toxic exposures, but the mechanism of this effect remained unknown (4). Our recent study demonstrates that the majority of Mn^{2+}-induced AKT is dependent on PI3K (28) (which also uses Mn^{2+} as a cofactor), however, PI3K and AKT can be activated via dozens of routes including receptor tyrosine kinases, integrins, cytokines, and G protein-coupled receptors (102, 103). Given the extensive crosstalk between Mn^{2+} and IGF observed in this study, we posited that Mn^{2+}-induced AKT signaling is mediated by IR/IGFR. We found that several IR/IGFR inhibitors with non-overlapping off-target kinases (Fig 5A) could inhibit the vast majority of Mn^{2+}-induced p-IGFR and p-AKT across every cell model tested (with the exception of HEK293 cells)— achieving ~50% inhibition of Mn^{2+}-induced p-AKT at approximate IC50 concentrations and >70% inhibition at higher concentrations (Fig 5, 6, 8, Supp Fig 6A–C). By correlating the degree of p-IGFR inhibition to p-AKT inhibition [(% of p-AKT inhibition) / (% of p-IGFR/IR inhibition)], we estimate that >70–80% of Mn^{2+}-induced p-AKT is dependent on p-IGFR in most cell lines (Supp Fig 6 B–C). Our observations strongly suggest that the vast majority of Mn^{2+}-induced AKT signaling in many cell types is mediated via interactions between Mn^{2+} and the insulin/IGF receptors themselves, rather than other upstream or downstream effectors.

Our data show that Mn^{2+} synergistically works with IR/IGFR to promote downstream AKT signaling, and that this is most likely due to the effects of intracellular, not extracellular, Mn^{2+} (Fig 9). Together, with the previously discussed inhibitor data (Fig 5, 8), we can narrow the initial site of action to the intracellular kinase domains of IGFR/IR (as these receptor-kinases do not require an upstream kinase for activation). As Mn^{2+} is a known cofactor for several other kinases, we postulated that Mn^{2+} is binding the kinase domain of IR/IGFR to stimulate receptor autophosphorylation and propagate signaling downstream. Our results are consistent with cell free in vitro experiments demonstrating the ability of

Mn^{2+} to act as a cofactor for these receptor and increase kinase activity in a defined biochemical system (61, 62). Future studies using structural crystallography or computational assessments could be performed to confirm that Mn^{2+} binds this intracellular region, but this will be challenging given the limited utility of available methods to detect Mn^{2+}-binding of proteins in living systems. Previous studies have shown that Mn^{2+} can stimulate insulin production itself to promote IGF signaling (51, 59). This study does not directly assess whether Mn^{2+} can increase insulin/IGF production, though our data suggest the mechanism of the Mn^{2+}-induced effect on IR/IGFR is derived from intracellular interactions, not interactions with the extracellular, ligand-binding, regions of the receptor (Fig 9). As the vast majority of Mn^{2+}-induced p-AKT is regulated by IR/IGFR, and Mn^{2+} is able to increase maximal AKT activity even under saturating concentrations of IGF, this also supports the hypothesis that Mn^{2+} is not acting at the ligand-binding domain or increasing the ligands themselves in our conditions/cell lines. However, we cannot exclude that Mn^{2+} may be able to promote insulin/IGF production or extracellular binding *in addition* to intracellular stimulation of the receptor itself.

Heavy metals, including Mn^{2+}, have specific proteins to which they bind, leading to activation of specific biological responses. However, excessive accumulation of cations can incur broad, non-specific activation of specific signaling cascades due to dyshomeostasis and toxicity. For instance, accumulation of many heavy metals will promote ROS production, broadly activating several signaling cascades (104, 105). In this study, we provide evidence that Mn^{2+}-induced IGF signaling is due to a highly specific interaction between Mn^{2+} and insulin/IGF receptors themselves, not merely a shared effect, such as ROS, by other cations (Fig 2A–C). This is supported by a previous study in which Mn^{2+}-induced p-AKT in the striatum was not blocked by antioxidant treatment, consistent with a ROS-independent mechanism (30). The concentrations we chose are the highest concentrations that these cells can be exposed to these cells for 24hrs without incurring detectable cell death (79). While Mn^{2+} can clearly activate p-AKT at sub-cytotoxic concentrations at 24hrs or during sub-acute, 7-day exposures (Fig 2A–F), it is possible that other metals could activate p-AKT at supra-toxic concentrations due to non-specific toxicity. A previous study in our lab observed that Cd could induce p-AKT at 50μM, which is a cytotoxic concentration of Cd (79). In this study, we used 20μM Cd which did not induce p-AKT. We posit that cytotoxic levels of Cu, Ni, Zn and other metals may also promote AKT signaling as this has been previously shown, though we did not detect any increase p-AKT induction by sub-toxic concentration of these metals (106–110).

Mn^{2+} and Mg^{2+} can compete for binding and activation of the same protein kinases. In fact, the vast majority of kinases in the human body are Mn^{2+}- and/or Mg^{2+}-dependent, though more often Mg^{2+}-dependent (111). Since DMEM-based media contains high physiological concentrations of Mg^{2+} to sustain enzymatic activity, we could not directly test whether Mg^{2+} could stimulate p-AKT alone. However, even in the presence of apparent saturating concentrations of Mg^{2+}, Mn^{2+} was still able to incur a ~3–4 fold increase in p-AKT after 24hrs in WT cells (Fig 1D,2B). Previous studies in a biochemically defined system reported the activation of the insulin receptor in the presence of Mg^{2+} or Mn^{2+}+Mg^{2+}. Our data demonstrate that Mn^{2+} can increase the maximal activity of the insulin/IGF receptors compared to Mg^{2+} alone in a living biological system as well. In this way, intracellular Mn^{2+}

could modulate maximal IGF signaling in a biological setting, even when sufficient Mg^{2+} is present in the cell. In the case of HD, reduced intracellular Mn^{2+} may cripple maximal IGF signaling and contribute to the AKT-related defects observed in HD, discussed more below.

Mn^{2+} is an essential cofactor for a variety of enzymes (1). Other studies, including our own, show that Mn^{2+} can incur activity of specific kinases and pathways that are not broadly shared by other metals (2, 3, 14, 57, 61, 63, 103, 112, 113) (Fig 2A–C). However, Mn^{2+} is not broadly recognized as a signaling molecule itself. We know that Mn^{2+} binds to and promotes activity of specific kinase pathways, but few studies have examined how biologically-relevant intracellular Mn^{2+} may help regulate cellular kinase activities, facilitating signaling cascades within the cell. Additionally, most studies have only examined the effect of Mn^{2+}-induced signaling at toxic concentrations of Mn^{2+}—here we demonstrate that Mn^{2+}-induced signaling can also occur at sub-cytotoxic concentrations. This suggests biologically-relevant concentrations of intracellular Mn^{2+} play a role in the normal signaling homeostasis of dozens of pathways. The discovery of a Mn^{2+}-specific chelator or small molecules that could manipulate intracellular Mn^{2+} could be incredibly beneficial in further elucidating the necessity of Mn^{2+} in cell signaling.

The AKT response to Mn^{2+} has also been associated with neuroprotection, as a way to stimulate pro-growth pathways (36, 42, 114–118). Here we observed that Mn^{2+} increased glucose uptake in STHdh HD cells only (Fig 10). While this increase was modest, it was also genotype-dependent, occurring only in a model of HD which exhibits reduced Mn^{2+} uptake and only at concentrations of Mn^{2+} which significantly increase p-AKT. We hypothesize, that under serum-deprived exposures (i.e. HBSS), Mn+IGF treatment may increase glucose uptake to a greater magnitude, perhaps even in WT cells, as Mn+IGF induces ~30-fold increases in p-AKT under these conditions (see Fig 1A), as opposed to 24hr exposures in media used in these experiments (see Fig 1D). This increase in glucose uptake is consistent with a role for AKT in promoting PFK1 phosphorylation and GLUT4 translocation to stimulate glucose uptake (102, 119). Since these glucose uptake experiments were done in serum-containing media, it is likely that glucose uptake (and upstream signaling) are at maximal homeostatic levels in WT cells (i.e. saturated with ligand, normal Mn uptake). We hypothesize that HD cells (possibly because of reduced insulin/IGF levels and/or reduced Mn-induced homeostasis/signaling) are unable to reach this maximal level. When cells are treated with Mn, this either 1) restores normal Mn bioavailability and downstream Mn-induced signaling or 2) compensates for a baseline, phenotypic decrease in insulin/IGF-induced p-AKT to increase glucose uptake. This suggests that Mn^{2+}, particularly in cases of reduced Mn^{2+} bioavailability, can stimulate neuroprotective processes, such as glucose uptake, which are impeded in neurodegenerative diseases like HD. This also demonstrates that Mn^{2+}-induced IGF signaling serves a role in mediating responsive, downstream biological processes, not merely just a broad response to higher intracellular Mn^{2+}. A number of studies have detected clear metabolic defects in glucose metabolism in HD 18F FDG PET imaging studies. Glucose hypometabolism has been detected in manifest HD patients in striatum and cortex and associated with motor and cognitive dysfunction, respectively(100, 120–123). Additionally, these defects have been found in patients prior to neuronal loss, suggesting glucose metabolism may be an early HD phenotype(124–126). Similarly, our studies have detected decreased Mn^{2+} uptake *in vivo*

only in prodromal (premanifest) mice. Given the results from our study, future studies should investigate whether Mn^{2+} uptake defects in vivo correlate temporally with perturbation in glucose uptake *in vivo* and whether Mn^{2+} treatment can remedy this.

Humbert and colleagues discovered that mutant HTT can be phosphorylated at Ser^{421} specifically by AKT, and this results in robust amelioration of cellular pathology, increasing cell survival and reducing aggregate accumulation (114, 127). Since then, other studies have examined the neuroprotective capacity of AKT stimulation more closely (84, 128, 129). Ahmed et al found that loss of IMPK, a mediator of PI3K and AKT activity, is disrupted in models of HD. However, overexpression of IMPK stimulated AKT activity and rescued cellular pathology and motor abnormalities in HD models, consistent with the neuroprotective potential of AKT. Similarly, we hypothesized, that in the context of reduced Mn^{2+} bioavailability (14, 79), suboptimal Mn^{2+} levels impair activation of IR/IGFR, reducing activity of AKT downstream and concurrently reducing the neuroprotective, pro-growth signaling that AKT provides to combat disease pathology. Of particular interest, Rego and colleagues have elucidated the neuroprotective effects of IGF treatment in cell and mouse models of HD, including upregulation of HTT Ser^{421} phosphorylation (65–67, 85, 130, 131). Additionally, Hiney and colleagues have shown that Mn^{2+} administration upregulates IGFR/AKT/Rheb/mTOR in vivo, which have been targeted to combat HD pathology in separate studies, providing a proof-of-principle that in vivo Mn^{2+} administration alone can potentiate IGF signaling in the brain (10, 132). Our study suggests Mn^{2+} can increase the maximal activity of the IGF signaling axis in living cells, even under saturating concentrations of IGF and Mg^{2+} (Fig 1D, 2A–C). Given the synergistic co-regulation of IGF and Mn^{2+} presented in this study, we hypothesize that co-treatment of HD models with Mn^{2+}+IGF may incur the greatest AKT stimulation and thus, increase the neuroprotective potential and therapeutic benefit of IGF-1 treatment alone.

Methods

Immortalized cell culture

The immortalized, murine striatal cell lines ($STHdh^{Q7/Q7}$ and STHdh $^{Q111/Q111}$ were obtained from Coriell Cell Repository (Cambden, NJ). STHdh striatal cells were cultured in Dulbecco's Modified Eagle Medium [D6546, Sigma-Aldrich, St. Louis MO] supplemented with 10% FBS [Atlanta Biologicals, Flowery Branch, GA], 2 mM GlutaMAX (Life Technologies, Carlsbad, CA), Penicillin-Streptomycin, 0.5 mg/mL G418 Sulfate (Life Technologies, Carlsbad, CA), MEM non-essential amino acids solution (Life Technologies, Carlsbad, CA), and 14mM HEPES (Life Technologies, Carlsbad, CA). They were incubated at 33°C and 5% CO_2. Cells were passaged before reaching greater than 90% confluency, and were never passaged past the recommended 14^{th} passage. The cells were split by trypsinization using 0.05% Trypsin-EDTA solution (Life Technologies, Carlsbad, CA) incubated for five minutes. One day prior to exposure, cells were plated in the appropriate cell culture plate type at 8×10^4 cells/mL for WT and 1×10^5 cell/mL for HD (as these HD cells grow slightly slower than WT counterparts). For some experiments, STHdh cells underwent serum deprivation in HBSS prior to exposures. For these, STHdh cells were plated the same as above. The day after, cells were wash 3X with HBSS and incubated for

one hour in HBSS. After this, treatments were added to the cells in HBSS for another 3 hours before lysates were collected for western blot.

For 1 week, low-dose Mn^{2+} exposures, STHdh cells were exposed to 0, 1, 5, or 10μM Mn^{2+}, 10 or 100nM IGF 24 hours after plating. The cells were split once, 1:4, midway through the week once they were near confluency. Exposure was continued with fresh media. Cells were harvested on day 7 at the same time of day as the original exposure day. Because of the original plating density difference, the density of Q7 and Q111 cells at the end of the 7 days was approximately equal.

NIH-3T3 and HEK293 cells were a generous gift from the Tansey lab. Cells were maintained and plated with high-glucose DMEM (Corning 0013CV) with penicillin-streptomycin. For experiments, they were plated at 100,000 cells/mL. After 48 hours, cell media was aspirated, cells were washed 1X with HBSS, and then fresh HBSS (without growth factors) was added for another hour to begin growth factor deprivation. After 1 hour of deprivation, media with IGF and/or Mn^{2+} and inhibitors was added to the cells for an additional 3 hours before protein lysates were collected.

Primary Rat Astrocyte cell culture

Primary cortical astrocytes were obtained according previous published protocols. Briefly, cortices of newborn Sprague-Dawley rats were carefully dissected and the meninges were removed(133, 134). Next, the cells were dissociated with a multi extraction protocol using dispase and DNAse and plated at 10,000 cells/cm^2 on poly-l-lysine coated dishes. The cells were maintained in minimum essential medium (MEM) supplemented with 10% horse serum, 100 U/ml penicillin and 100 μg/ml streptomycin. The first media exchanged occurred 24 hours after plating the cells, and after that once every 3–4 days. After 7–8 days in culture, the cells reached confluence and the astrocytes were used for the respective experiments.

hiPSC cell culture

Three control and HD-patient derived hiPSC-lines were differentiated into striatal islet-1-positive neuroprogenitor cells as previously described (14). HD patient mutant alleles were 58, 66, and 70 CAG repeats. All hiPSC lines were confirmed to be pluripotent (PluriTest-Expression Analysis, Durham, NC) and to have normal karyotypes (Genetics Associates, Nashville, TN). Additionally, a subset of cells was fixed with 4% paraformaldehyde for 15 minutes and immunocytochemistry was performed to ensure all cultures expressed the striatal marker Islet-1.

For experiments, striatal neurprogenitor cells were plated at 300,000 cells/mL at day 10 of differentiation. At day 11, purmorphamine and rock inhibitor-containing media was replaced with fresh media containing purmorphamine (.65μM) for 24hrs. For 3-hour exposures, cells were washed with HBSS 3X and then cells underwent growth factor/insulin deprivation in media without N2 supplement (which contains the insulin for the differentiation media) for 3 hours. This was followed by exposing the cells in N2 supplement-free media with Mn^{2+}, inhibitors, and IGF-1 for another 3 hours prior to protein collection. Other N2 components include human transferrin, progesterone, putrescine, and selenite.

In order to test the effects of intracellular vs extracellular Mn^{2+}, cells were exposed to 200 or 500 μM Mn^{2+} for 3hrs in -N2 media 24hrs after removing rock inhibitor containing media. After, cells were washed 3 times with HBSS and then replaced with IGF-containing -N2 media for another 3 hours prior to protein collection. -N2 media without IGF was added to half the wells to ascertain the effect of IGF alone.

Inhibitors/growth factors/metals

Inhibitors/growth factors were used at the following concentrations: recombinant human IGF-1 (R+D systems Cat# 291-G1)= .1–10μM, recombinant human EGF protein (R+D systems Cat# 236-EG), BMS-53692436924 (SelleckChem)= 100nM-1μM, BMS-7548075480754807 (SelleckChem)= 2nM, Linsitinib (SelleckChem)= 100nm-1μM, NVP-AEW541 (SellekChem)= 100nM-1μM, and LY294002 (Tocris)= 7μM.

The following metallic compounds were used as sources for the metal exposures: $MnCl_2 \cdot 4H_2O$ (Sigma Aldrich, St. Louis, MO) for Mn^{2+}, $FeCl_3$ (Sigma Aldrich, St. Louis, MO) as Fe^{3+}, : $CuCl_2 \cdot 2H_2O$ (Alfa Aesar, Ward Hill, MA) for Cu^{2+}, $MgCl_2 \cdot 6H_2O$ (Alfa Aesar, Ward Hill, MA) for Mg^{2+}, $ZnCl_2$ (Acros Organics, Morris, NJ) for Zn^{2+}, $CdCl_2 \cdot H_2O$ (for Cd, $NiCl_2 \cdot 6H_2O$ (Alfa Aesar, Ward Hill, MA) for Ni^{2+}, and $CoCl_2 \cdot 6H_2O$ (MP Biomedicals, Solon, OH) for Co^{2+} exposures.

Western blot

Cells were washed once with ice cold PBS and then scraped from wells of a 6-well plate directly into 100ul, ice-cold RIPA buffer containing protease inhibitor (Sigma-Aldrich, St. Louis, MO) and phosphatase inhibitor cocktails 2 & 3 (Sigma, Sigma-Aldrich, St. Louis, MO). Cell lysates were centrifuged at 4°C for 10 minutes at 20,000 *g*. Protein concentration was quantified using the BCA assay (Peirce Technologies). Samples were mixed with 5x SDS loading buffer containing 1% 2-mercaptoethanol and boiled for 5 minutes. Fifteen μg of protein was loaded for each sample onto a 4–20% pre-cast gel SDS-PAGE gel (BioRad, Hercules, CA) and run at 90V for 120 minutes. The protein bands were then transferred onto nitrocellulose membranes using iBlot Gel Transfer Device (Life Technologies). The remaining gel was stained with Coomassie Blue stain (Biorad, Hercules, CA). Since the gels retained ~1/3 of the original protein after transferring with the iBlot, we imaged the stained gel on the Li-Cor Odyssey Imaging System and quantified the intensity entire lane from ~150–20 kDa. This value was used to normalize the quantification of the immunostained bands. The membrane was blocked in Odyssey Blocking Buffer for one hour prior to the addition of the primary antibodies. The primary antibodies were diluted 1:1000 in Odyssey Blocking Buffer containing 0.1% TWEEN and incubated overnight. After washing three times for 5 minutes in TBST, membranes were incubated with secondary antibodies at 1:10,000 (LiCor, Lincoln, NE) for 1 hour. Following three, 5-minute washes in TBST, membranes were imaged using the Li-Cor Odyssey Imaging System, and quantification was performed using Image Studio Lite (LiCOR, Lincoln, NE). In Figure 6A, membranes were visualized using CL-XPosure film (Thermo Scientific, #34090) and quantified via ImageJ.

pIR/IGFR Tyr^{1135} (3918), pan IR/IGFR (9750), p-AKT Ser^{473} (4060), p-AKT Thr^{308} (2965), pan AKT (2920), and pan S6 (2317), p-S6 $Ser^{235/236}$ (2211) antibodies were

purchased from cell signaling technologies and used at 1:1000 dilution except pIR/IGFR was used at 1:500. Note: Unless stated, all western blots examined p-AKT at the Ser^{473} residue. All blots aside from Figure 6A were normalized by total protein (Coomassie). Figure 6A was quantified at p-AKT over actin. Pan protein expression was quantified separately in the Supplemental Figure 1, 4 as it did not significantly change under our exposure paradigms. Additionally, a direct comparison showing lack of a significant differences between phosphorylated expression of proteins normalized to pan protein expression or to Coomassie (total protein) for STHdh and Islet cells can be found in Supplemental Figure 7.

Note: Many of our experiments were performed to maximize the number of conditions/genotypes/cell lines/exposure time and, thus most replicates of western blots included conditions that were not relevant for specific figure panels. Thus, some western blot images were cut to exclude these non-relevant conditions. However, any western blots that are grouped together for any specific figure panel come from a single blot and are only cut/copied to exclude unneeded conditions/replicates for simplicity and space.

Cellular Fura-2 Manganese Uptake Assay (CFMEA) was performed as described previously(86).

PC12 cell HTT induction and differentiation

HTT PC12 cells were purchased from Coriell Repositories (CH00285, CH00287, CH00289). Undifferentiated cells were plated at 75,000 cell/mL in DMEM F12 media with 4.5 g/L glucose, L-glutamine, and sodium pyruvate with 10% fetal bovine serum, 5% horse serum, 250ug/mL zeocin (Invitrogen), 100ug/mL G418, and 1% penstrep. Cells were plated on collagen-coated plates at 75,000 cells/mL. Cells were induced with 5μM ponasterone A (Invitrogen) and differentiated with 50ng/uL neural growth factor (NGF- Cell signaling technologies) for 6 days prior to exposures. On the 6^{th} day, exposures were added for an additional 24 hours with ponasterone A. Cells were imaged by microscopy for neurite outgrowth and expression of RFP-HTT, assuring induction and differentiation of cultures.

qRT-PCR for IR/IGFR/IRS2

STHdh Q7/Q7 and Q111/Q111 cells were plated in 6-well plates and treated with Mn^{2+} and/or IGF-1. After 24 hours, cells were lysed in 1mL of TRIzol® Reagent (CatNo. 15596) and stored at -80°C until use. Total RNA was extracted using TRIzol® Reagent, according to the manufacturer's User Guide (Invitrogen, Carlsbad, CA). RNA was DNAse I treated, following the NEB DNase I Reaction Protocol (M0303) (New England BioLabs® Inc, Ipswich, MA). cDNA was generated on Bio-Rad Laboratories' S1000™ Thermal Cycler, using 50μM Random Hexamers (P/N 100026484, Invitrogen, Carlsbad, CA), 50U MuLV Reverse Transcriptase (P/N 100023379, Applied Biosystems, Foster City, CA), 10mM dNTPs (CatNo. N0446S, NEB, Ipswich, MA), 20U RNAse, Inhibitor (CatNo. N8080119, Applied Biosystems, Foster City, CA), 25mM $MgCl_2$ (P/N100020476, Applied Biosystems, Foster City, CA), 10x PCR Buffer II (RefNo. 4486220 Applied Biosystems by Life Technologies, Austin, TX), and 1ug of extracted RNA, and using the following cycling times: 25°C for 10 min, 42°C for 60 min, 99°C for 5 min, 5°C for 5 min, 4°C forever. Q-RT-

PCR was performed on Eppendorf's Mastercycler® epGradientS Realplex^2, using KAPA SYBR® FAST qPCR Master Mix (2X) Universal according to the manufacturer's recommendations (KM4101, KAPA Biosystems, Wilmington, MA). Sequences of primers used are as follows: *mpgk1*_R2 AAAGGCCATTCCACCACCAA, *mpgk1*_F2 GCTATCTTGGGAGGCCTAA, *Irs2* forward, GTCCAGGCACTGGAGCTTT, *Irs2* reverse, GCTGGTAGCGCTTCACTCTT, IGFR For Primer GCTTCTGTGAACCCCGAGTATTT, IGFR Rev Primer TGGTGATCTTCTCTCGAGCTACCT, IR For Primer TTTGTCATGGATGGAGGCTA, IR Rev Primer CCTCATCTTGGGGTTGAACT.

Glucose uptake assay

Glucose Uptake-Glo Assay was conducted per manufacturer instructions (Promega, Madison, WI). Q7 and Q111 cells were cultured after plating for 16–24 hours in 96-well tissue plates. 24 hours prior to the Glucose Uptake-Glo Assay, the media was removed and replaced with media containing 0, 50, or 100μM Mn^{2+}. The, the media was removed and the wells washed with 100μl PBS. 50μl of prepared 1mM 2DG was added per well, plates were briefly shaken, and incubated for 10 minutes at room temperature. The, 25μl of Stop Buffer was added and the plate briefly shaken again. Thereafter, 25μl of Neutralization Buffer was added to each well and the plate shaken briefly. This was followed by addition of 100μl of 2DG6P Detection Reagent to each well, the plate was briefly shaken and then incubated for 30 minutes at 33 degrees (the normal temperature for these cell lines). Luminescence was recorded using a 0.3–1 second integration on a microplate reader (BioTek Synergy H1, Winooski, VT).

Statistical analysis

GraphPad Prism version 8.0.2 was used. Most data are shown by fold change to increase clarity for the reader. However, all data that was analyzed by one-way or two-way ANOVA was converted to log values to allow for a normal distribution for the statistical analysis. For any data comparing values versus a unitary value (=1) on a graph- raw, unnormalized data was converted to log values and underwent ANOVA analysis to maintain normal distribution. Data was then often plotted as normalized values for ease of review. If data sets were significant by ANOVA, post-hoc multiple comparisons tests were used to determine specific differences within data sets. For analyses across all possible treatments/genotypes, Tukey's test was performed. For analyses comparing data back to a specific condition only, Dunnet's or Sidak's tests were performed. For the majority of data sets, paired analyses were used as all samples were collected as full sets. For the data sets which compared two points specifically, a paired student's t-test was used as indicated.

Supplementary Material

Refer to Web version on PubMed Central for supplementary material.

Acknowledgements:

We would like to thank Dr. A. Cristina Rego for formative and insightful discussion of insulin signaling in HD. We would also like to thank many other members of the Bowman lab including Dr. Anna Pfalzer, Dr. Emily Warren, Dr. Diana Neely, Dr. Terry Jo Bichell, Dr. Bingying Han, Kyle Horning, Jordyn Wilcox, and Yueli Zhang, Ilyana Ilieva, for technical expertise and for thoughtful assistance with experimental design and interpretation.

Funding:

NIH/NIEHS RO1 ES010563 (ABB, MA) and RO1 ES016931 (ABB). NIH/NIEHS F31 ES028084 (MRB). VBI Scholars Program, NIH/NIEHS 5T32 ES7028-44 (PJ).

References

1. Horning KJ, Caito SW, Tipps KG, Bowman AB, Aschner M, Manganese Is Essential for Neuronal Health. Annual review of nutrition 35, 71–108 (2015).
2. Chan DW et al., Purification and characterization of ATM from human placenta. A manganese-dependent, wortmannin-sensitive serine/threonine protein kinase. The Journal of biological chemistry 275, 7803–7810 (2000). [PubMed: 10713094]
3. Sato T, Nakashima A, Guo L, Tamanoi F, Specific Activation of mTORC1 by Rheb G-protein in Vitro Involves Enhanced Recruitment of Its Substrate Protein. Journal of Biological Chemistry 284, 12783–12791 (2009). [PubMed: 19299511]
4. Bae J-H et al., Manganese induces inducible nitric oxide synthase (iNOS) expression via activation of both MAP kinase and PI3K/Akt pathways in BV2 microglial cells. Neuroscience letters 398, 151–154 (2006). [PubMed: 16417967]
5. Cai T et al., Manganese Induces Tau Hyperphosphorylation through the Activation of ERK MAPK Pathway in PC12 Cells. Toxicological Sciences 119, 169–177 (2011). [PubMed: 20937724]
6. Crittenden PL, Filipov NM, Manganese modulation of MAPK pathways: effects on upstream mitogen activated protein kinase kinases and mitogen activated kinase phosphatase-1 in microglial cells. Journal of applied toxicology : JAT 31, 1–10 (2011). [PubMed: 20589745]
7. Exil V et al., Activation of MAPK and FoxO by manganese (Mn) in rat neonatal primary astrocyte cultures. PloS one 9, (2014).
8. Jang B-CC, Induction of COX-2 in human airway cells by manganese: role of PI3K/PKB, p38 MAPK, PKCs, Src, and glutathione depletion. Toxicology in vitro : an international journal published in association with BIBRA 23, 120–126 (2009). [PubMed: 19084589]
9. McDougall SA, Der-Ghazarian T, Britt CE, Varela FA, Crawford CA, Postnatal manganese exposure alters the expression of D2L and D2S receptor isoforms: relationship to PKA activity and Akt levels. Synapse (New York, N.Y.) 65, 583–591 (2011).
10. Srivastava VK, Hiney JK, Dees WL, Manganese-Stimulated Kisspeptin Is Mediated by the IGF-1/Akt/Mammalian Target of Rapamycin Pathway in the Prepubertal Female Rat. Endocrinology 157, 3233–3241 (2016). [PubMed: 27309941]
11. Hirata Y, Adachi K, Kiuchi K, Activation of JNK pathway and induction of apoptosis by manganese in PC12 cells. Journal of neurochemistry 71, 1607–1615 (1998). [PubMed: 9751194]
12. Hirata Y, Adachi K, Kiuchi K, Phosphorylation and activation of p70 S6 kinase by manganese in PC12 cells. Neuroreport 9, 3037–3040 (1998). [PubMed: 9804312]
13. Tai Y, Chew KCM, Tan BWQ, Lim K-L, Soong T, Iron mitigates DMT1-mediated manganese cytotoxicity via the ASK1-JNK signaling axis: Implications of iron supplementation for manganese toxicity. Scientific Reports 6, 21113 (2016). [PubMed: 26878799]
14. Tidball AM et al., A novel manganese-dependent ATM-p53 signaling pathway is selectively impaired in patient-based neuroprogenitor and murine striatal models of Huntington's disease. Human Molecular Genetics 24, 1929–1944 (2015). [PubMed: 25489053]
15. Moreno JA, Streifel KM, Sullivan KA, Hanneman WH, Tjalkens RB, Manganese-Induced NF-κB Activation and Nitrosative Stress Is Decreased by Estrogen in Juvenile Mice. Toxicological Sciences 122, 121–133 (2011). [PubMed: 21512103]
16. Wang L et al., The effect of postnatal manganese exposure on the NMDA receptor signaling pathway in rat hippocampus. Journal of Biochemical and Molecular Toxicology 31, (2017).
17. Perl DP, Olanow WC, The Neuropathology of Manganese-Induced Parkinsonism. Journal of Neuropathology & Experimental Neurology 66, 675–682 (2007). [PubMed: 17882011]
18. Kwakye GF, Paoliello M, Mukhopadhyay S, Bowman AB, Aschner M, Manganese-Induced Parkinsonism and Parkinson's Disease: Shared and Distinguishable Features. International Journal of Environmental Research and Public Health 12, 7519–7540 (2015). [PubMed: 26154659]

19. Olanow CW, Manganese-Induced Parkinsonism and Parkinson's Disease. Annals of the New York Academy of Sciences 1012, 209–223 (2004). [PubMed: 15105268]
20. Tong M, Dong M, de la Monte SM, Brain insulin-like growth factor and neurotrophin resistance in Parkinson's disease and dementia with Lewy bodies: potential role of manganese neurotoxicity. Journal of Alzheimer's disease : JAD 16, 585–599 (2009). [PubMed: 19276553]
21. Takeda A, Manganese action in brain function. Brain Research Reviews 41, 79–87 (2003). [PubMed: 12505649]
22. Dieter HH, Bayer TA, Multhaup G, Environmental Copper and Manganese in the Pathophysiology of Neurologic Diseases (Alzheimer's Disease and Manganism). Acta hydrochimica et hydrobiologica 33, 72–78 (2005).
23. Park RM, Neurobehavioral Deficits and Parkinsonism in Occupations with Manganese Exposure: A Review of Methodological Issues in the Epidemiological Literature. Safety and Health at Work 4, 123–135 (2013). [PubMed: 24106642]
24. Nagatomo S et al., Manganese intoxication during total parenteral nutrition: report of two cases and review of the literature. Journal of the Neurological Sciences 162, 102–105 (1999). [PubMed: 10064179]
25. Lucchini RG et al., Tremor, olfactory and motor changes in Italian adolescents exposed to historical ferromanganese emission. NeuroToxicology 33, 687–696 (2012). [PubMed: 22322213]
26. McDougall SA, Der-Ghazarian T, Britt CE, Varela FA, Crawford CA, Postnatal manganese exposure alters the expression of D2L and D2S receptor isoforms: Relationship to PKA activity and Akt levels. Synapse 65, 583–591 (2011). [PubMed: 21484877]
27. Cordova FM et al., In Vivo Manganese Exposure Modulates Erk, Akt and Darpp-32 in the Striatum of Developing Rats, and Impairs Their Motor Function. PLoS ONE 7, (2012).
28. Bryan MR et al., Phosphatidylinositol 3 kinase (PI3K) modulates manganese homeostasis and manganese-induced cell signaling in a murine striatal cell line. NeuroToxicology, (2017).
29. Cheng H et al., PI3K/Akt signaling pathway and Hsp70 activate in hippocampus of rats with chronic manganese sulfate exposure. Journal of Trace Elements in Medicine and Biology, (2018).
30. Cordova FM et al., Manganese-exposed developing rats display motor deficits and striatal oxidative stress that are reversed by Trolox. Archives of toxicology 87, 1231–1244 (2013). [PubMed: 23385959]
31. Acevedo-Torres K et al., Mitochondrial DNA damage is a hallmark of chemically induced and the R6/2 transgenic model of Huntington's disease. DNA Repair 8, 126–136 (2009). [PubMed: 18935984]
32. Duarte AI et al., IGF-1 protects against diabetic features in an in vivo model of Huntington's disease. Experimental Neurology 231, 314–319 (2011). [PubMed: 21763311]
33. Guan J et al., N-terminal tripeptide of IGF-1 (GPE) prevents the loss of TH positive neurons after 6-OHDA induced nigral lesion in rats. Brain research 859, 286–292 (2000). [PubMed: 10719076]
34. Offen D et al., Protective effect of insulin-like-growth-factor-1 against dopamine-induced neurotoxicity in human and rodent neuronal cultures: possible implications for Parkinson's disease. Neuroscience letters 316, 129–132 (2001). [PubMed: 11744219]
35. Ebert AD, Beres AJ, Barber AE, Svendsen CN, Human neural progenitor cells over-expressing IGF-1 protect dopamine neurons and restore function in a rat model of Parkinson's disease. Experimental neurology 209, 213–223 (2007). [PubMed: 18061591]
36. Quesada A, Lee BY, Micevych PE, PI3 kinase/Akt activation mediates estrogen and IGF-1 nigral DA neuronal neuroprotection against a unilateral rat model of Parkinson's disease. Developmental neurobiology 68, 632–644 (2008). [PubMed: 18278798]
37. Godau J, Herfurth M, Kattner B, Gasser T, Berg D, Increased serum insulin-like growth factor 1 in early idiopathic Parkinson's disease. Journal of neurology, neurosurgery, and psychiatry 81, 536–538 (2010).
38. Bassil F, Fernagut P-O, Bezard E, Meissner WG, Insulin IGF-1 and GLP-1 signaling in neurodegenerative disorders: Targets for disease modification? Progress in Neurobiology 118, 1–18 (2014). [PubMed: 24582776]

39. Pellecchia MT et al., Insulin-like growth factor-1 predicts cognitive functions at 2-year follow-up in early, drug-naïve Parkinson's disease. European Journal of Neurology 21, 802–807 (2014). [PubMed: 23551560]
40. Lee J-M et al., Identification of Genetic Factors that Modify Clinical Onset of Huntington's Disease. Cell 162, 516–526 (2015). [PubMed: 26232222]
41. Bernhard FP et al., Insulin-Like Growth Factor 1 (IGF-1) in Parkinson's Disease: Potential as Trait-, Progression- and Prediction Marker and Confounding Factors. PLOS ONE 11, (2016).
42. Ayadi AE, Zigmond MJ, Smith AD, IGF-1 protects dopamine neurons against oxidative stress: association with changes in phosphokinases. Experimental brain research 234, 1863–1873 (2016). [PubMed: 26894890]
43. Busiguina S et al., Neurodegeneration is associated to changes in serum insulin-like growth factors. Neurobiology of disease 7, 657–665 (2000). [PubMed: 11114263]
44. Gasparini L, Xu H, Potential roles of insulin and IGF-1 in Alzheimer's disease. Trends in Neurosciences 26, 404–406 (2003). [PubMed: 12900169]
45. Torres-Aleman I, Targeting insulin-like growth factor-1 to treat Alzheimer's disease. Expert opinion on therapeutic targets 11, 1535–1542 (2007). [PubMed: 18020976]
46. Freude S, Schilbach K, Schubert M, The role of IGF-1 receptor and insulin receptor signaling for the pathogenesis of Alzheimer's disease: from model organisms to human disease. Current Alzheimer research 6, 213–223 (2009). [PubMed: 19519303]
47. Moloney AM et al., Defects in IGF-1 receptor, insulin receptor and IRS-1/2 in Alzheimer's disease indicate possible resistance to IGF-1 and insulin signalling. Neurobiology of aging 31, (2010).
48. Neill C, PI3-kinase/Akt/mTOR signaling: impaired on/off switches in aging, cognitive decline and Alzheimer's disease. Experimental gerontology 48, 647–653 (2013). [PubMed: 23470275]
49. Johansson P et al., Serum but not cerebrospinal fluid levels of insulin-like growth factor-I (IGF-I) and IGF-binding protein-3 (IGFBP-3) are increased in Alzheimer's disease. Psychoneuroendocrinology 38, 1729–1737 (2013). [PubMed: 23473966]
50. Keen CL, Baly DL, Lönnerdal B, Metabolic effects of high doses of manganese in rats. Biological Trace Element Research 6, 309–315 (1984). [PubMed: 24264109]
51. Baly DL, Effect of Manganese Deficiency on Insulin Secretion and Carbohydrate Heomostasis in Rats. J.Nutrition, (1984).
52. Baly DL, Keen CL, Hurley LS, Effects of manganese deficiency on pyruvate carboxylase and phosphoenolpyruvate carboxykinase activity and carbohydrate homeostasis in adult rats. Biological Trace Element Research 11, 201–212 (1986). [PubMed: 24254514]
53. Baly DL, Lee I, Doshi R, Mechanism of decreased insulinogenesis in manganese-deficient rats. Decreased insulin mRNA levels. FEBS letters 239, 55–58 (1988). [PubMed: 2460371]
54. Baly DL, Schneiderman JS, Garcia-Welsh AL, Effect of manganese deficiency on insulin binding, glucose transport and metabolism in rat adipocytes. The Journal of nutrition 120, 1075–1079 (1990). [PubMed: 2204694]
55. Clegg MS et al., The influence of manganese deficiency on serum IGF-1 and IGF binding proteins in the male rat. Proceedings of the Society for Experimental Biology and Medicine. Society for Experimental Biology and Medicine (New York, N.Y.) 219, 41–47 (1998).
56. Subasinghe S, Greenbaum AL, McLean P, The insulin-mimetic action of Mn2+: involvement of cyclic nucleotides and insulin in the regulation of hepatic hexokinase and glucokinase. Biochemical medicine 34, 83–92 (1985). [PubMed: 2996512]
57. Morrison BD, Feltz SM, Pessin JE, Polylysine specifically activates the insulin-dependent insulin receptor protein kinase. The Journal of biological chemistry 264, 9994–10001 (1989). [PubMed: 2542339]
58. Hiney JK, Srivastava VK, Dees WL, Manganese induces IGF-1 and cyclooxygenase-2 gene expressions in the basal hypothalamus during prepubertal female development. Toxicological sciences : an official journal of the Society of Toxicology 121, 389–396 (2011). [PubMed: 21402727]
59. Lee S-H et al., Manganese Supplementation Protects Against Diet-Induced Diabetes in Wild Type Mice by Enhancing Insulin Secretion. Endocrinology 154, 1029–1038 (2013). [PubMed: 23372018]

60. Ueda M, Robinson FW, Smith MM, Kono T, Effects of divalent cations on the regulation of insulin-sensitive glucose transport and cAMP phosphodiesterase in adipocytes. Insulin-like effects of divalent cations. The Journal of biological chemistry 259, 9520–9525 (1984). [PubMed: 6086637]

61. Mooney RA, Green DA, Insulin receptor dephosphorylation in permeabilized adipocytes is inhibitable by manganese and independent of receptor kinase activity. Biochemical and Biophysical Research Communications 162, 1200–1206 (1989). [PubMed: 2475105]

62. Xu B, Bird VG, Miller WT, Substrate specificities of the insulin and insulin-like growth factor 1 receptor tyrosine kinase catalytic domains. The Journal of biological chemistry 270, 29825–29830 (1995). [PubMed: 8530377]

63. Singh TJ, Activation of a manganese-dependent membrane protein kinase by serine and tyrosine phosphorylation. Biochemical and biophysical research communications 171, 75–83 (1990). [PubMed: 1697468]

64. Lopes C et al., IGF-1 intranasal administration rescues Huntington's disease phenotypes in YAC128 mice. Molecular neurobiology 49, 1126–1142 (2014). [PubMed: 24347322]

65. Ribeiro M, Rosenstock TR, Oliveira AM, Oliveira CR, Rego AC, Insulin and IGF-1 improve mitochondrial function in a PI-3K/Akt-dependent manner and reduce mitochondrial generation of reactive oxygen species in Huntington's disease knock-in striatal cells. Free radical biology & medicine 74, 129–144 (2014). [PubMed: 24992836]

66. Naia L et al., Activation of IGF-1 and insulin signaling pathways ameliorate mitochondrial function and energy metabolism in Huntington's Disease human lymphoblasts. Molecular neurobiology 51, 331–348 (2015). [PubMed: 24841383]

67. Naia L et al., Insulin and IGF-1 regularize energy metabolites in neural cells expressing full-length mutant huntingtin. Neuropeptides, (2016).

68. Yamamoto A, Cremona ML, Rothman JE, Autophagy-mediated clearance of huntingtin aggregates triggered by the insulin-signaling pathway. The Journal of cell biology 172, 719–731 (2006). [PubMed: 16505167]

69. Podolsky S, Leopold N, Sax D, INCREASED FREQUENCY OF DIABETES MELLITUS IN PATIENTS WITH HUNTINGTON'S CHOREA. The Lancet 299, 1356–1359 (1972).

70. Farrer LA, Diabetes mellitus in Huntington disease. Clinical genetics 27, 62–67 (1985). [PubMed: 3156696]

71. Hurlbert MS et al., Mice transgenic for an expanded CAG repeat in the Huntington's disease gene develop diabetes. Diabetes 48, 649–651 (1999). [PubMed: 10078572]

72. Dexter DT et al., ALTERATIONS IN THE LEVELS OF IRON, FERRITIN AND OTHER TRACE METALS IN PARKINSON'S DISEASE AND OTHER NEURODEGENERATIVE DISEASES AFFECTING THE BASAL GANGLIA. Brain 114, 1953–1975 (1991). [PubMed: 1832073]

73. Rosas DH et al., Cerebral cortex and the clinical expression of Huntington's disease: complexity and heterogeneity. Brain 131, 1057–1068 (2008). [PubMed: 18337273]

74. Rosas DH et al., Alterations in Brain Transition Metals in Huntington Disease: An Evolving and Intricate Story. Archives of Neurology 69, 887–893 (2012). [PubMed: 22393169]

75. Williams BB et al., Altered manganese homeostasis and manganese toxicity in a Huntington's disease striatal cell model are not explained by defects in the iron transport system. Toxicological sciences : an official journal of the Society of Toxicology 117, 169–179 (2010). [PubMed: 20547568]

76. Kwakye GF, Li D, Bowman AB, Novel high-throughput assay to assess cellular manganese levels in a striatal cell line model of Huntington's disease confirms a deficit in manganese accumulation. NeuroToxicology 32, 630–639 (2011). [PubMed: 21238486]

77. Madison JL, Wegrzynowicz M, Aschner M, Bowman AB, Disease-toxicant interactions in manganese exposed Huntington disease mice: early changes in striatal neuron morphology and dopamine metabolism. PloS one 7, (2012).

78. Bichell TV et al., Reduced bioavailable manganese causes striatal urea cycle pathology in Huntington's disease mouse model. Biochimica et Biophysica Acta (BBA) - Molecular Basis of Disease 1863, 1596–1604 (2017). [PubMed: 28213125]

79. Williams BB et al., Disease-toxicant screen reveals a neuroprotective interaction between Huntington's disease and manganese exposure. Journal of neurochemistry 112, 227–237 (2010). [PubMed: 19845833]
80. Pfalzer AC, Wages PA, Porter NA, Bowman AB, Striatal Cholesterol Precursors Are Altered with Age in Female Huntington's Disease Model Mice. Journal of Huntington's disease, (2019).
81. Talbot K et al., Demonstrated brain insulin resistance in Alzheimer's disease patients is associated with IGF-1 resistance, IRS-1 dysregulation, and cognitive decline. The Journal of clinical investigation 122, (2012).
82. Bowman AB, Aschner M, Considerations on manganese (Mn) treatments for in vitro studies. NeuroToxicology 41, 141–142 (2014). [PubMed: 24509086]
83. Colin E et al., Akt is altered in an animal model of Huntington's disease and in patients. The European journal of neuroscience 21, 1478–1488 (2005). [PubMed: 15845076]
84. Zala D et al., Phosphorylation of mutant huntingtin at S421 restores anterograde and retrograde transport in neurons. Human Molecular Genetics 17, 3837–3846 (2008). [PubMed: 18772195]
85. Lopes C et al., IGF-1 intranasal administration rescues Huntington's disease phenotypes in YAC128 mice. Molecular neurobiology 49, 1126–1142 (2014). [PubMed: 24347322]
86. Tidball AM et al., A novel manganese-dependent ATM-p53 signaling pathway is selectively impaired in patient-based neuroprogenitor and murine striatal models of Huntington's disease. Human molecular genetics 24, 1929–1944 (2015). [PubMed: 25489053]
87. Boucher J, Tseng Y-H, Kahn RC, Insulin and Insulin-like Growth Factor-1 Receptors Act as Ligand-specific Amplitude Modulators of a Common Pathway Regulating Gene Transcription. Journal of Biological Chemistry 285, 17235–17245 (2010). [PubMed: 20360006]
88. Boucher J, Kleinridders A, Kahn RC, Insulin Receptor Signaling in Normal and Insulin-Resistant States. Cold Spring Harbor Perspectives in Biology 6, (2014).
89. Wittman M et al., Discovery of a (1H-benzoimidazol-2-yl)-1H-pyridin-2-one (BMS-536924) inhibitor of insulin-like growth factor I receptor kinase with in vivo antitumor activity. Journal of medicinal chemistry 48, 5639–5643 (2005). [PubMed: 16134929]
90. Wittman MD et al., Discovery of a 2,4-disubstituted pyrrolo[1,2-f][1,2,4]triazine inhibitor (BMS-754807) of insulin-like growth factor receptor (IGF-1R) kinase in clinical development. Journal of medicinal chemistry 52, 7360–7363 (2009). [PubMed: 19778024]
91. Mulvihill MJ et al., Discovery of OSI-906: a selective and orally efficacious dual inhibitor of the IGF-1 receptor and insulin receptor. Future Medicinal Chemistry 1, 1153–1171 (2009). [PubMed: 21425998]
92. Garcıá-Echeverrıá C et al., In vivo antitumor activity of NVP-AEW541—A novel, potent, and selective inhibitor of the IGF-IR kinase. Cancer Cell 5, 231–239 (2004). [PubMed: 15050915]
93. Reddy HP, Mao P, Manczak M, Mitochondrial structural and functional dynamics in Huntington's disease. Brain research reviews 61, 33–48 (2009). [PubMed: 19394359]
94. Ferreira LI et al., Bioenergetic dysfunction in Huntington's disease human cybrids. Experimental Neurology 231, 127–134 (2011). [PubMed: 21684277]
95. Josefsen K et al., Impaired glucose tolerance in the R6/1 transgenic mouse model of Huntington's disease. Journal of neuroendocrinology 20, 165–172 (2007). [PubMed: 18034868]
96. Acuña AI et al., A failure in energy metabolism and antioxidant uptake precede symptoms of Huntington's disease in mice. Nature Communications 4, 2917 (2013).
97. Mochel F, Haller RG, Energy deficit in Huntington disease: why it matters. Journal of Clinical Investigation 121, 493–499 (2011). [PubMed: 21285522]
98. Morea V et al., Glucose transportation in the brain and its impairment in Huntington disease: one more shade of the energetic metabolism failure? Amino Acids 49, 1147–1157 (2017). [PubMed: 28396959]
99. Browne SE, Beal FM, The Energetics of Huntington's Disease. Neurochemical Research 29, 531–546 (2004). [PubMed: 15038601]
100. Ciarmiello A et al., 18F-FDG PET uptake in the pre-Huntington disease caudate affects the time-to-onset independently of CAG expansion size. European Journal of Nuclear Medicine and Molecular Imaging 39, 1030–1036 (2012). [PubMed: 22526956]

101. Yan H et al., Circulating IGF1 regulates hippocampal IGF1 levels and brain gene expression during adolescence. Journal of Endocrinology 211, 27–37 (2011). [PubMed: 21750148]
102. Manning BD, Cantley LC, AKT/PKB signaling: navigating downstream. Cell 129, 1261–1274 (2007). [PubMed: 17604717]
103. Chauhan V, Singh SS, Chauhan A, Brockerhoff H, Phosphatidylinositol 3-kinase: Inhibition of intrinsic protein-serine kinase activity by phosphoinositides, and of lipid kinase activity by Mn2+. Biochimica et Biophysica Acta (BBA) - Molecular Cell Research 1267, 139–144 (1995). [PubMed: 7612667]
104. Milatovic D et al., Manganese Induces Oxidative Impairment in Cultured Rat Astrocytes. Toxicological Sciences 98, 198–205 (2007). [PubMed: 17468184]
105. Milatovic D, Zaja-Milatovic S, Gupta RC, Yu Y, Aschner M, Oxidative damage and neurodegeneration in manganese-induced neurotoxicity. Toxicology and Applied Pharmacology 240, 219–225 (2009). [PubMed: 19607852]
106. Pan J et al., Reactive Oxygen Species-Activated Akt/ASK1/p38 Signaling Pathway in Nickel Compound-Induced Apoptosis in BEAS 2B Cells. Chemical Research in Toxicology 23, 568–577 (2010). [PubMed: 20112989]
107. Li J et al., Nickel Compounds Act through Phosphatidylinositol-3-kinase/Akt-Dependent, p70S6k-Independent Pathway to Induce Hypoxia Inducible Factor Transactivation and Cap43 Expression in Mouse Epidermal Cl41 Cells. Cancer Research 64, 94–101 (2004). [PubMed: 14729612]
108. Ostrakhovitch EA, Lordnejad M, Schliess F, Sies H, Klotz L-O, Copper Ions Strongly Activate the Phosphoinositide-3-Kinase/Akt Pathway Independent of the Generation of Reactive Oxygen Species. Archives of Biochemistry and Biophysics 397, 232–239 (2002). [PubMed: 11795876]
109. Barthel A, Ostrakhovitch EA, Walter PL, Kampkötter A, Klotz L-O, Stimulation of phosphoinositide 3-kinase/Akt signaling by copper and zinc ions: Mechanisms and consequences. Archives of Biochemistry and Biophysics 463, 175–182 (2007). [PubMed: 17509519]
110. Tang X, Shay NF, Zinc has an insulin-like effect on glucose transport mediated by phosphoinositol-3-kinase and Akt in 3T3-L1 fibroblasts and adipocytes. The Journal of nutrition 131, 1414–1420 (2001). [PubMed: 11340092]
111. Bidlack WR, The Biological Chemistry of Magnesium Edited by J. A. Cowan (The Ohio State University). VCH Publishers, Inc.: New York. 1995. xvi + 254 pp. $59.95. ISBN 1–56081-627–9. Journal of the American Chemical Society 118, 6–7 (1996).
112. Lovitt B et al., Differential effects of divalent manganese and magnesium on the kinase activity of leucine-rich repeat kinase 2 (LRRK2). Biochemistry 49, 3092–3100 (2010). [PubMed: 20205471]
113. Maydan M et al., Integrin-Linked Kinase Is a Functional Mn2+-Dependent Protein Kinase that Regulates Glycogen Synthase Kinase-3β (GSK-3β) Phosphorylation. PLoS ONE 5, (2010).
114. Humbert S et al., The IGF-1/Akt Pathway Is Neuroprotective in Huntington's Disease and Involves Huntingtin Phosphorylation by Akt. Developmental Cell 2, 831–837 (2002). [PubMed: 12062094]
115. Aberg DN, Brywe K, Isgaard J, Aspects of growth hormone and insulin-like growth factor-I related to neuroprotection, regeneration, and functional plasticity in the adult brain. TheScientificWorldJournal 6, 53–80 (2006).
116. Fang X-X, Jiang X-L, Han X-H, Peng Y-P, Qiu Y-H, Neuroprotection of Interleukin-6 Against NMDA-induced Neurotoxicity is Mediated by JAK/STAT3, MAPK/ERK, and PI3K/AKT Signaling Pathways. Cellular and Molecular Neurobiology 33, 241–251 (2013). [PubMed: 23161148]
117. Blázquez C et al., The CB_1 cannabinoid receptor signals striatal neuroprotection via a PI3K/Akt/mTORC1/BDNF pathway. Cell death and differentiation 22, 1618–1629 (2015). [PubMed: 25698444]
118. Zhao Q, Ye J, Wei N, Fong C, Dong X, Protection against MPP+-induced neurotoxicity in SH-SY5Y cells by tormentic acid via the activation of PI3-K/Akt/GSK3β pathway. Neurochemistry International 97, 117–123 (2016). [PubMed: 26994872]

119. Whiteman EL, Cho H, Birnbaum MJ, Role of Akt/protein kinase B in metabolism. Trends in Endocrinology & Metabolism 13, 444–451 (2002). [PubMed: 12431841]
120. Antonini A et al., Striatal glucose metabolism and dopamine D2 receptor binding in asymptomatic gene carriers and patients with Huntington's disease. Brain 119, 2085–2095 (1996). [PubMed: 9010012]
121. Kuwert T et al., CORTICAL AND SUBCORTICAL GLUCOSE CONSUMPTION MEASURED BY PET IN PATIENTS WITH HUNTINGTON'S DISEASE. Brain 113, 1405–1423 (1990). [PubMed: 2147116]
122. Young AB et al., PET scan investigations of Huntington's disease: Cerebral metabolic correlates of neurological features and functional decline. Annals of Neurology 20, 296–303 (1986). [PubMed: 2945510]
123. Berent S et al., Positron emission tomographic scan investigations of Huntington's disease: Cerebral metabolic correlates of cognitive function. Annals of Neurology 23, 541–546 (1988). [PubMed: 2970247]
124. Hayden MR et al., Positron emission tomography in the early diagnosis of Huntington's disease. Neurology 36, 888–888 (1986). [PubMed: 2940474]
125. Ciarmiello A et al., Brain white-matter volume loss and glucose hypometabolism precede the clinical symptoms of Huntington's disease. Journal of nuclear medicine : official publication, Society of Nuclear Medicine 47, 215–222 (2006).
126. Feigin A et al., Metabolic network abnormalities in early Huntington's disease: an [(18)F]FDG PET study. Journal of nuclear medicine : official publication, Society of Nuclear Medicine 42, 1591–1595 (2001).
127. Humbert S, Saudou F, Huntingtin phosphorylation and signaling pathways that regulate toxicity in Huntington's disease. Clinical Neuroscience Research 3, 149–155 (2003).
128. Gauthier LR et al., Huntingtin Controls Neurotrophic Support and Survival of Neurons by Enhancing BDNF Vesicular Transport along Microtubules. Cell 118, 127–138 (2004). [PubMed: 15242649]
129. Metzler M et al., Phosphorylation of Huntingtin at Ser421 in YAC128 Neurons Is Associated with Protection of YAC128 Neurons from NMDA-Mediated Excitotoxicity and Is Modulated by PP1 and PP2A. The Journal of Neuroscience 30, 14318–14329 (2010). [PubMed: 20980587]
130. Weydt P et al., Thermoregulatory and metabolic defects in Huntington's disease transgenic mice implicate PGC-1α in Huntington's disease neurodegeneration. Cell Metabolism 4, 349–362 (2006). [PubMed: 17055784]
131. Duarte AI, Proença T, Oliveira CR, Santos MS, Rego AC, Insulin restores metabolic function in cultured cortical neurons subjected to oxidative stress. Diabetes 55, 2863–2870 (2006). [PubMed: 17003354]
132. Lee JH et al., Reinstating aberrant mTORC1 activity in Huntington's disease mice improves disease phenotypes. Neuron 85, 303–315 (2014). [PubMed: 25556834]
133. Culbreth M, Zhang Z, Neurotoxicology A-M, Methylmercury augments Nrf2 activity by downregulation of the Src family kinase Fyn. Neurotoxicology, (2017).
134. Allen JW, Mutkus LA, Aschner M, Isolation of neonatal rat cortical astrocytes for primary cultures. Current protocols in toxicology 4, (2000).

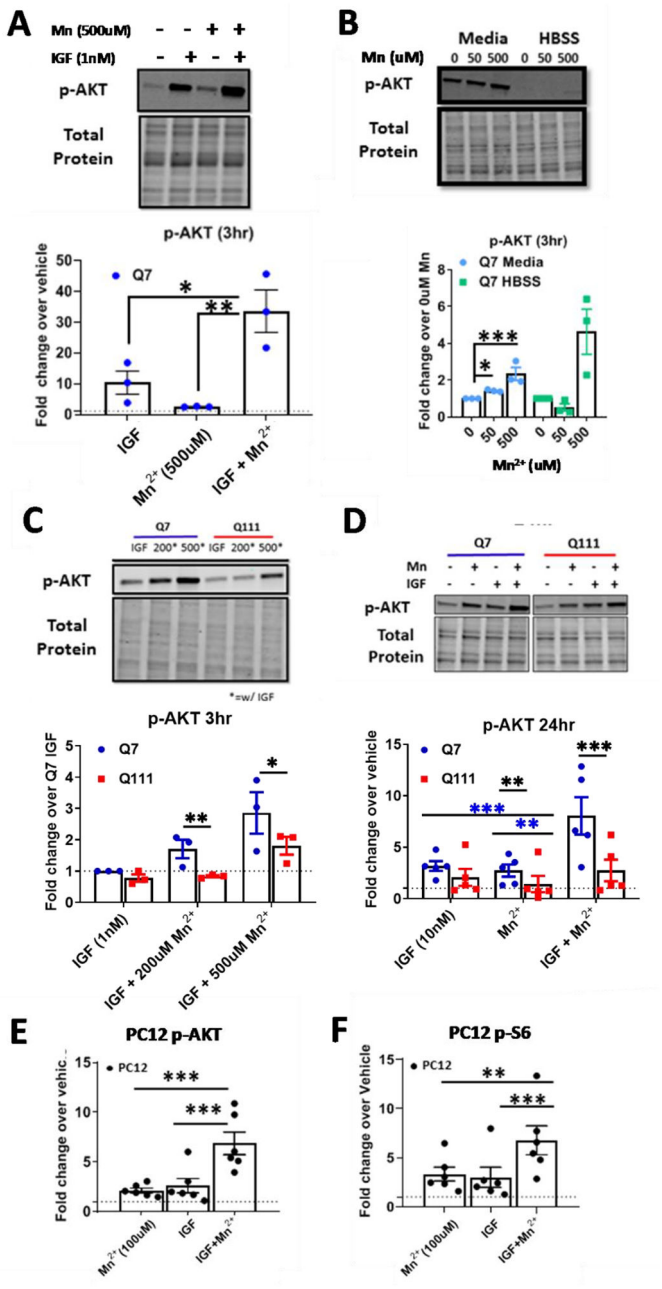

Figure 1: Mn^{2+} can potentiate IGF-1 induced p-AKT and Mn^{2+}-induced p-AKT is reduced in HD cells.

A) p-AKT expression in STHdh Q7/Q7 following a 1hr serum deprivation, then 3hr exposure in HBSS with 1nM IGF-1 and/or 500μM Mn^{2+}. Vehicle=dotted line. One-way ANOVA; treatment= F(2,6)=20.12; p=0.0022. **B)** Quantification of p-AKT after 3hr, 50/500μM Mn^{2+} exposure in serum free HBSS (following 1hr serum deprivation) or media containing 10% FBS. Two-way ANOVA; treatment= F(2,6)=40.84; p=0.0003; media/ HBSS= F(1,3)= 671.6; p=0.0001; treatment-media interaction= F(2,6)= 24,37; p=0.0013. **C)** p-AKT expression in STHdh WT and HD cells following 1hr serum deprivation then 3hr Mn^{2+} (0/200/500μM) + IGF (1nM) exposure in HBSS. Two-way ANOVA; treatment= F(2,

4)= 10.29; p=0.0265. **D)** p-AKT expression after 24hrs treatment with 10nM IGF-1, 50μM Mn^{2+}, or both in STHdh Q7/Q7 and Q111/Q111. Two-way ANOVA; treatment= F(2,10)=40.84; p=0.0064; genotype= F(1,5)= 671.6; p=0.0163; treatment-genotype interaction= F(2,10)= 1.587; p=0.2515. **E,F**) p-AKT (Ser^{473}) and p-S6 ($Ser^{235/236}$) in uninduced PC12 cells following treatment with 100μM Mn^{2+}, 10nM IGF-1, or both. For these PC12 experiments, all uninduced (i.e. were only expressing WT rat HTT) samples from the 23Q, 74Q, and 140Q (3 biological replicates each) were used. Representative blot Supp Fig 1C. One-way ANOVA; p-AKT treatment= F(2,10)=36.71; p=<0.0001; One-way ANOVA; p-S6 treatment= F(2,10)=20.57; p=<0.0003; Error bars= SEM. Dotted line= vehicle (=1). N=3 for Panel A-C; N=4 for panel D; N=5 for panel E; N=6 for panels F and G. *= significant by Tukey's (A, F, G), Dunnet (B), and Sidak multiple comparison (D-E). *P<.05, **P<.01, ***P<.001.

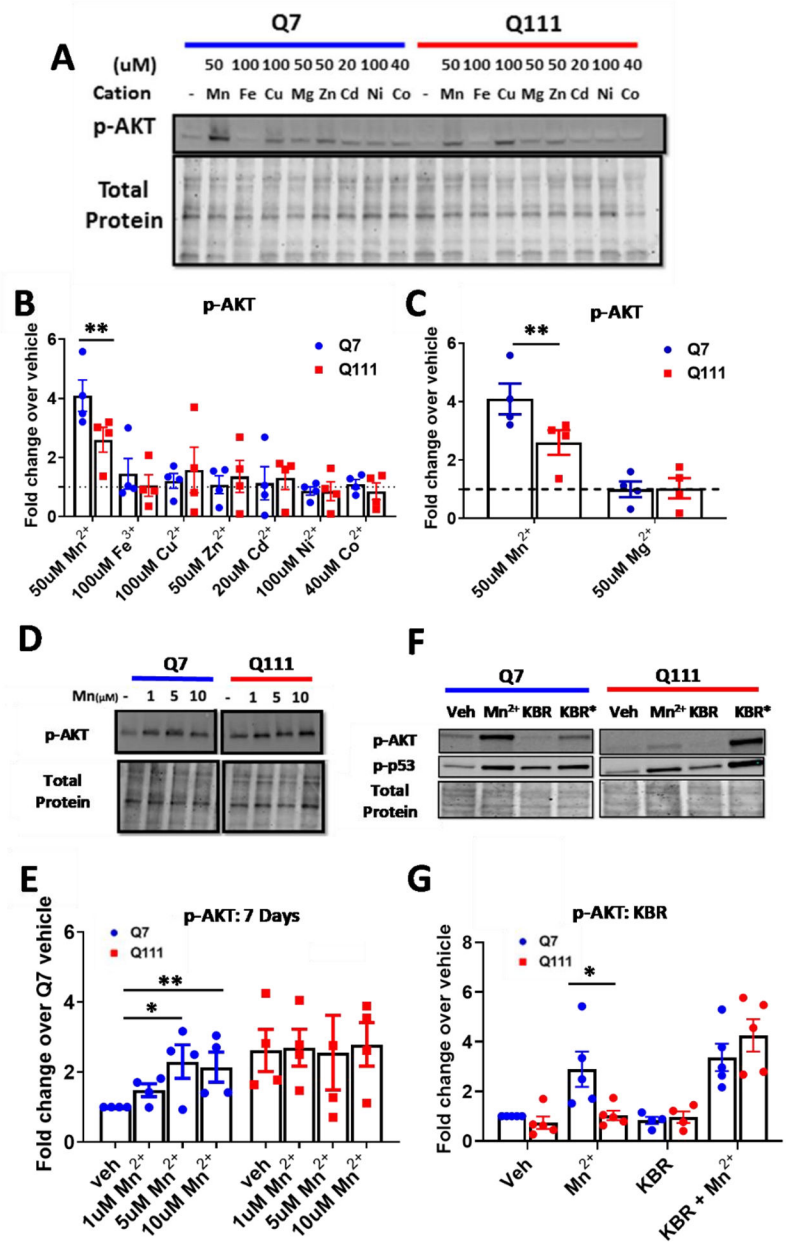

Figure 2: Assessing the specificity and dynamics of the Mn^{2+}-AKT interaction.

A) Representative blot for p-AKT expression in STHdh Q7/Q7 and Q111/Q111 cells following 24hr exposures with Mn^{2+}, Fe^{3+}, Cu^{2+}, Mg^{2+}, Zn^{2+}, Cd^{2+}, Ni^{2+}, or Co^{2+}. **B**) Quantification of p-AKT expression, blot shown in panel A. **C**) Quantification of only Mn^{2+} and Mg^{2+}-induced p-AKT after 24hrs, blot shown in panel A. Two-way ANOVA; treatment= $F(8, 24)=2.509$; $p=<0.0388$. N=4; Error bars= SEM; Normalized to respective vehicle. **D**) Representative blot for p-AKT and p-S6 expression in STHdh Q7/Q7 and Q111/Q111 cells following 7-day exposure with Mn^{2+} (1/5/10μM) or IGF (10nM). **E**) Quantification of p-AKT expression, blot shown in panel D. N=4. Error=SEM. Two-way ANOVA; treatment= $F(3,9)=.5284$; $p=0.6738$; genotype= $F(1,3)= 33.39$; $p=0.0103$; treatment-genotype interaction= $F(3,9)= 4.912$; $p=0.0273$. **F**) Representative blot for p-AKT

and p-p53 expression following 24hr exposure with 50μM Mn^{2+}, 10μM KB-R7943, or both. **G**) Quantification of p-AKT expression, blot shown in panel H (p-p53 quantification not shown). Two-way ANOVA; treatment= F(3,12)=24.91; p=<0.0001; genotype= F(1,4)= 2.840 p=0.1672; treatment-genotype interaction= F(3,12)= 4.761; p=0.0207. N=4; Error bars= SEM. *= significant by Dunnet (B, C, E), and Sidak multiple comparison tests (G,H). *P<.05, **P<.01, ***P<.001.

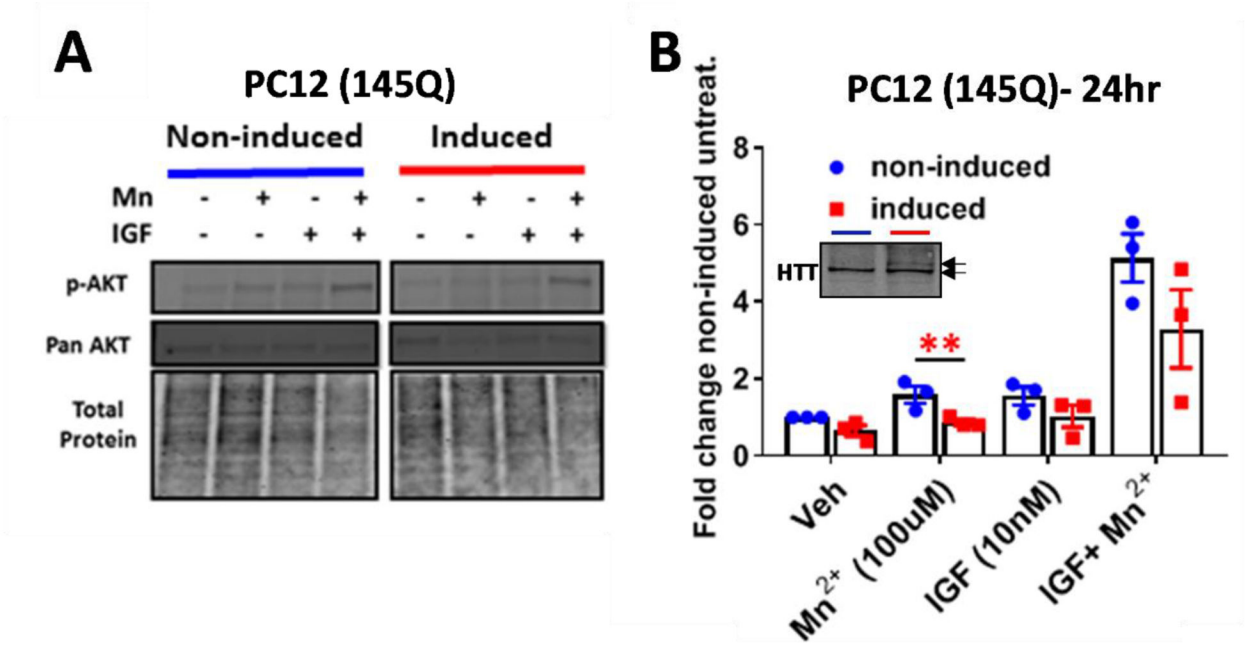

Figure 3: Assessing the effects of WT and mutant HTT in Mn^{2+}-induced pAKT.

A) Representative western blot of PC12 cells in differentiated and 145Q HTT-induced PC12 cells following 24hr exposure with 100μM Mn^{2+} and/or IGF (10nM) **B**) Quantification of p-AKT expression. 145Q induced HTT cells (red) are compared to uninduced counterparts (blue). Image of WT HTT (bottom arrow) and 145Q HTT (top arrow) expression using mAb 2166 inset within graph- blue= non-induced, red= induced. N=3; Error bars= SEM, *= significance genotype difference by student's t-test. *P<.05, **P<.01, ***P<.001.

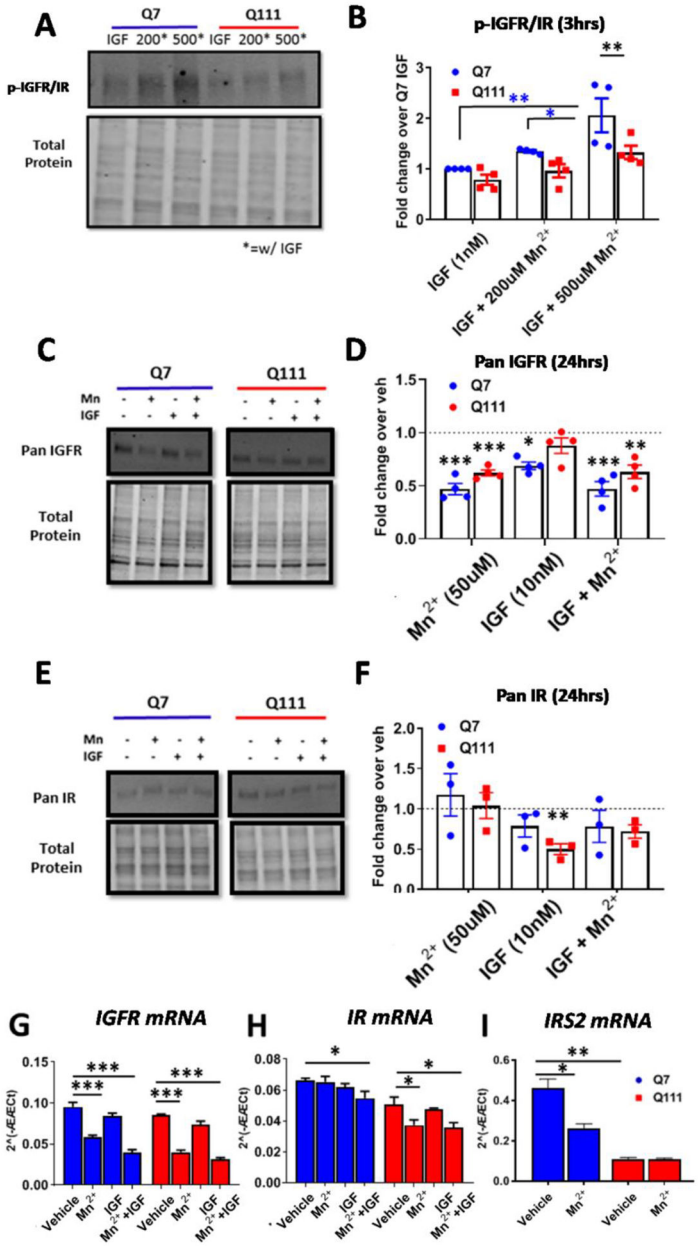

Figure 4: Mn^{2+} increases phosphorylation of IR/IGFR and decreases total protein and mRNA expression.

A,B) Representative western blot and quantification of p-IGFR expression in STHdh cells following 1hr serum deprivation and 3hr Mn^{2+} (200/500μM) + IGF(1nM) exposures. Note representative blot is the same samples/run as Figure 1C. Two-way ANOVA; treatment= F(2,6)=5.461; p=<0.0446; genotype= F(1,3)= 30.98; p=0.0114; treatment-genotype interaction= F(2,6)= 3.275; p=0.1093. N=4. **C,D**) Representative western blot and quantification of pan IGFR protein expression in STHdh cells following 24hr exposure with Mn^{2+} (50μM) and/or IGF (10nM). Dotted line= Vehicle (=1). Two-way ANOVA for IGFR; treatment= F(3,9)=16.71; p=<0.0005. N=4. **E,F)** Representative western blot and quantification of pan IR protein expression in STHdh cells following 24hr exposure with

Mn^{2+} (50μM) and/or IGF (10nM). Dotted line= Vehicle (=1). Two-way ANOVA for IR; treatment= F(3,6)=20.59; p=0.0015. N=3. **G-I)** mRNA expression of IGFR (**G**), IR (**H**), and IRS2 (**I**) after 24hr Mn^{2+} (50μM) and/or IGF (10nM) exposure. Two-way ANOVA treatment for IGFR: F(3,6)=85.01; p=<0.0001. For IR: F(3,6)=7.204; p=<0.0205. For IRS2: F(1,3)=213.8; p=<0.0007.Error bars= SEM; N=4 for panels A-D, G-I; N=3 for E,F. P<.05, **P<.01, ***P<.001. *= significant by Tukey's (B) or Dunnet's (D, F, G, H, I) multiple comparison tests.

A

Inhibitor Reference	IC50 nM	Known Off-targets	Concentrations Used
BMS-536924 [89]	100 (IGFR), 73 (IR)	FAK, MEK, LCK	100nM, 1uM
BMS-754807 [90]	1.8 (IGFR), 1.7 (IR)	Trk, Met, Ron, Aurora	2nM, 10nM
NVP-AEW541 [92]	150 (IGFR), 140 (IR)	FLT1/3, TEK	100nM, 1uM
Linsitinib (OSI-906) [91]	35 (IGFR), 75 (IR)	IRR	100nM, 1uM

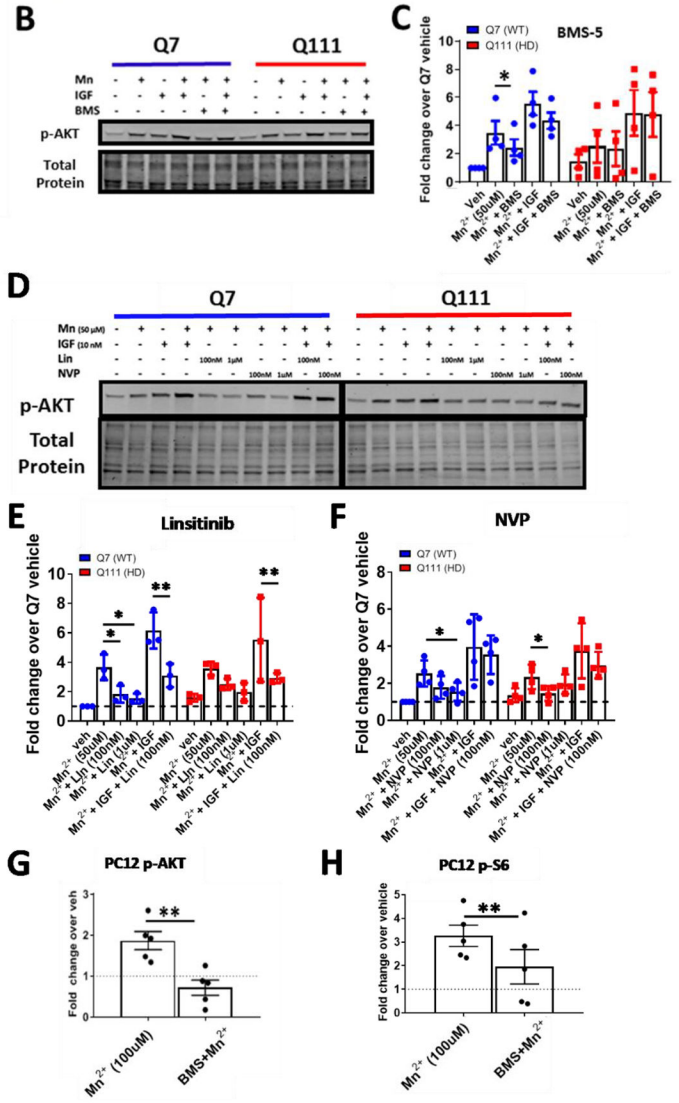

Figure 5: IR/IGFR inhibitors block Mn^{2+}-induced p-AKT.

A) List of IR/IGFR inhibitor names, IC50s for IR/IGFR, off-targets, and concentrations used here. **B**) Representative western blot of pAKT expression STHdh Q7/Q7 and Q111/Q111 after 24hr treatment with Mn^{2+} (50μM), IGF (10nM), and/or BMS-536924 (100nM).**C**) Quantification of Mn^{2+}/IGF induced p-AKT expression with BMS536924 (100nM). Two-way ANOVA for BMS5 treatment; F(1.610, 4.831)=20.03; p=.0039. N=4. **D**) Representative western blot of p-AKT expression in STHdh Q7/Q7 and Q111/Q111 after 24hr treatment with Mn^{2+} (50μM), Linsitinib (100nm/1μM), NVP-AEW541-AEW541 (100nM/1μM) and Mn^{2+}+IGF(10nM). **E, F**) Quantification of Mn^{2+}/IGF-induced p-AKT expression with Linsitinib (**E**) or NVP-AEW541 (**F**) Two-way ANOVA for LLinsitinib treatment; F(4,8)=8.414; p=.0182; Two-way ANOVA for NVP treatment; F(4,8)=10.68; p=.0027. N=3–

4. **G, H**) Quantification of p-AKT (**G**) and p-S6 (**H**) expression in uninduced PC12 cells treated with 100μM Mn^{2+} or Mn^{2+} (100μM) + BMS536924 (100nM) after 24hr exposures. Representative blot Supp Fig 1C. *= significance by student's t-test. For these PC12 experiments, uninduced samples from the 23Q, 74Q, and 140Q (total N=5) were used. Note representative blot Supplemental Fig 1C. Error bars= SEM. Dotted line= Vehicle (=1). *P<.05, **P<.01, ***P<.001.

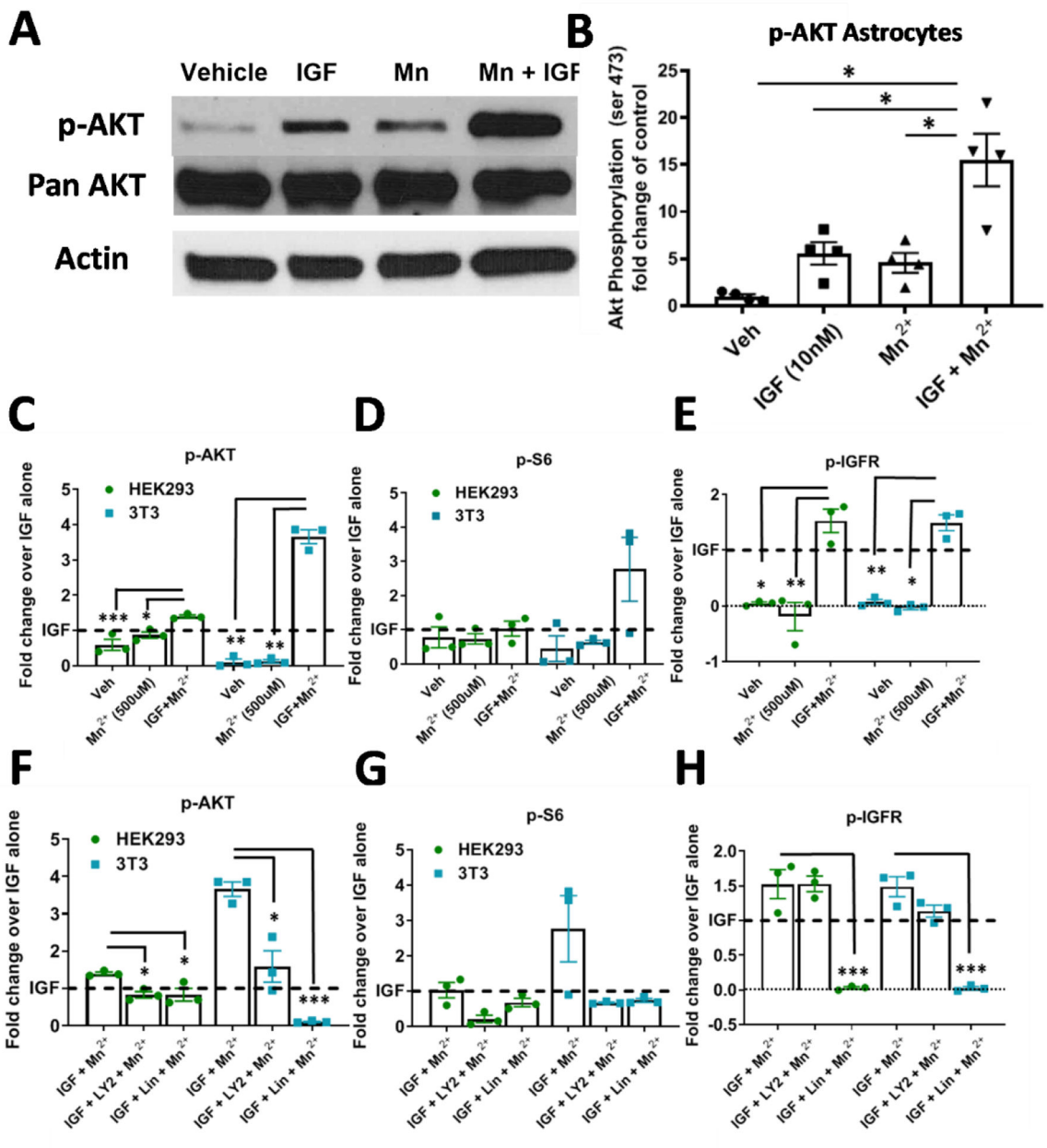

Figure 6: Mn^{2+} increases p-AKT and p-IGFR expression in the presence of IGF-1 in astrocytes and non-neuronal cell lines.

A, B) Representative western blot and quantification of p-AKT in astrocytes after 1hr serum deprivation followed by 3hr exposure with Mn^{2+} (500μM), IGF (1nM), or both. One-way ANOVA; treatment= F(1.167, 3.501)=24.37; p=<0.0104. N=4. Error= SEM. **C-E)** Quantifications of western blots of 3T3 and HEK293 p-AKT (**C**) p-S6 (**D**), p-IGFR (**E**) expression after 1hr serum deprivation followed by 3hr exposure in HBSS with Mn^{2+} (100μM), IGF (1nM), or both. **F-H)** Quantifications of western blots of 3T3 and HEK293 p-AKT (**F**), p-S6 (**G**), p-IGFR (**H**) expression after 1hr serum deprivation followed by 3hr exposure in HBSS with Mn^{2+} (100μM) + IGF (1nM) with LY294002 (7μM), and/or LLinsitinib (1μM). Representative blot in Supp. Fig 3. N=3; Error bars= SEM; Dotted line=

IGF alone (=1). One-way ANOVA for p-IGFR; HEK: F(1.284, 2.568)= 38.12; p=.0129; 3T3: F(1.221, 2.442)=99.63; p=.0048. One-way ANOVA for p-AKT; HEK: F(4,8)= 9.391; p=.0041; 3T3: F(4,8)=8.544; p=.0055. One-way ANOVA for p-S6; HEK: F(1.274, 2.548)= 5.081; p=.1270; 3T3: F(1.014, 2.028)=3.123; p=.2180 *= significance by Dunnet's multiple comparison test.*P<.05, **P<.01, ***P<.001.

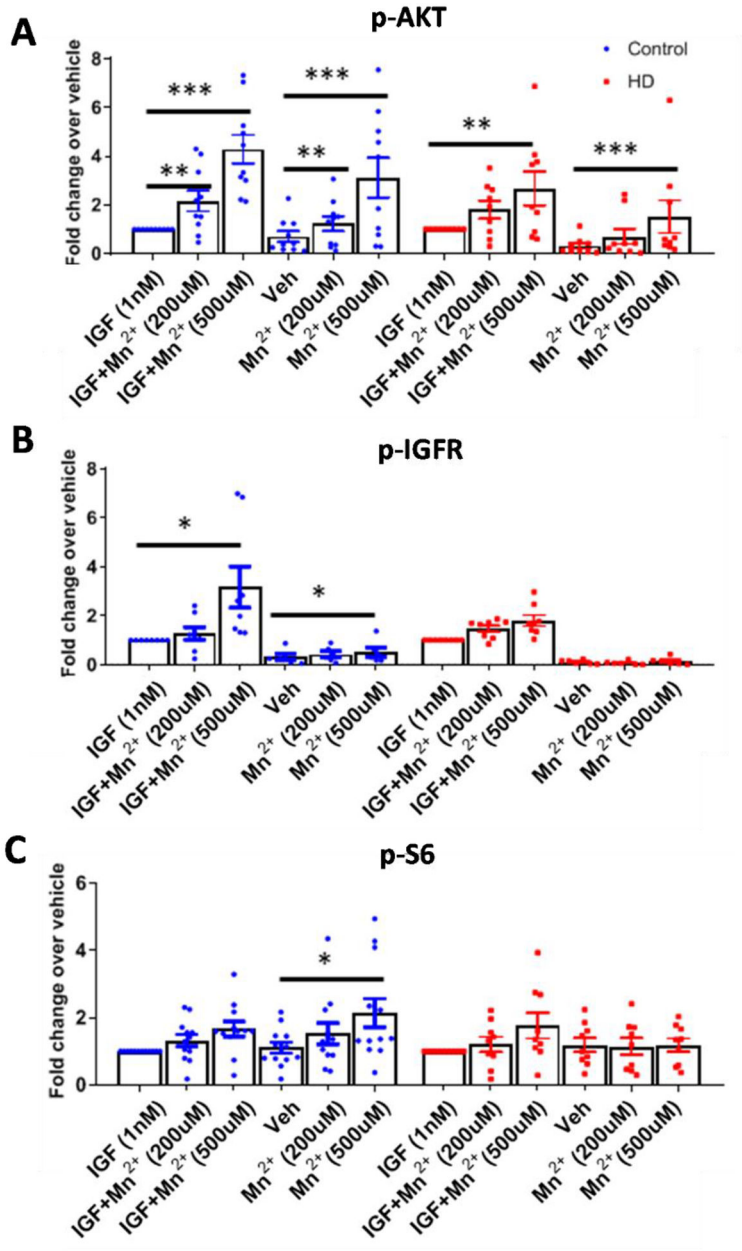

Figure 7: Mn^{2+}-induced p-AKT, IGFR is reduced in HD hiPSC-derived neuroprogenitors.

A-C) Western blot quantification of hiPSC-derived neuroprogenitors from three control patients and three HD patients (CAG repeat 58, 66, 70) for p-AKT (**A**), p-IGFR (**B**), and p-S6 (**C**), following treatment 3hr treatment with Mn^{2+} (200/500μM) or Mn^{2+}+IGF (1nM) in growth factor/insulin free media, after 3hr serum deprivation. N=8–12 for control from three separate patients, N=7–9 for HD including three separate patients; Error bars= SEM. All data normalized to respective control or HD treated IGF-1 alone. Representative blot in Supplemental Fig 5A,B. One-way ANOVA stats listed in Supp Fig 4D. *= significance from vehicle by Dunnet's multiple comparison test. *P<.05, **P<.01, ***P<.001.

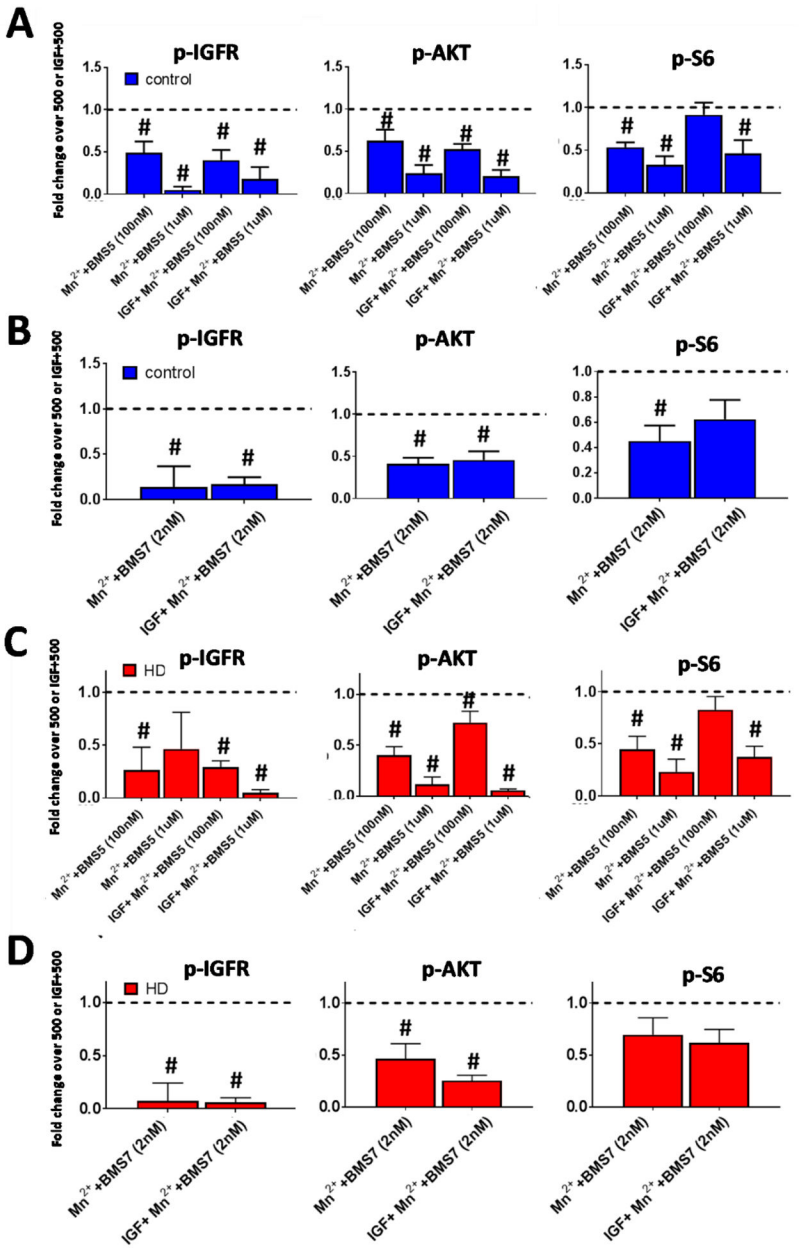

Figure 8: Mn^{2+}-induced p-AKT, IGFR is blocked by IR/IGFR inhibition in HD hiPSC-derived neuroprogenitors.

Western blot quantification of control and HD patient iPSC-derived neuroprogenitors following treatment 3hr treatment with Mn^{2+} (500μM) or Mn^{2+}+IGF (1nM) in growth factor/insulin free media, after 3hr N2 supplement (insulin/growth factor) withdrawal. **A-D)** Quantification of p-IGFR, p-AKT, and p-S6 in control (Blue, **A**,**B**) or HD (Red, **C**,**D**) after treatment with BMS-536924 (100nM/1μM; **A,C**) or BMS-754807 (2nM; **B,D**). All data is represented as fold change compared to Mn^{2+} alone or Mn^{2+}+IGF (both normalized=1). Samples were from the exact same patient cell lines and differentiations as Figure 7. N=4–6 per condition across three control and three HD patients. Representative blot in

Supplemental Fig 5.A,B. #= significant difference to Veh (dotted line=1 for -IGF conditions) or IGF alone (dotted line=1 for +IGF conditions) by 95% CI.

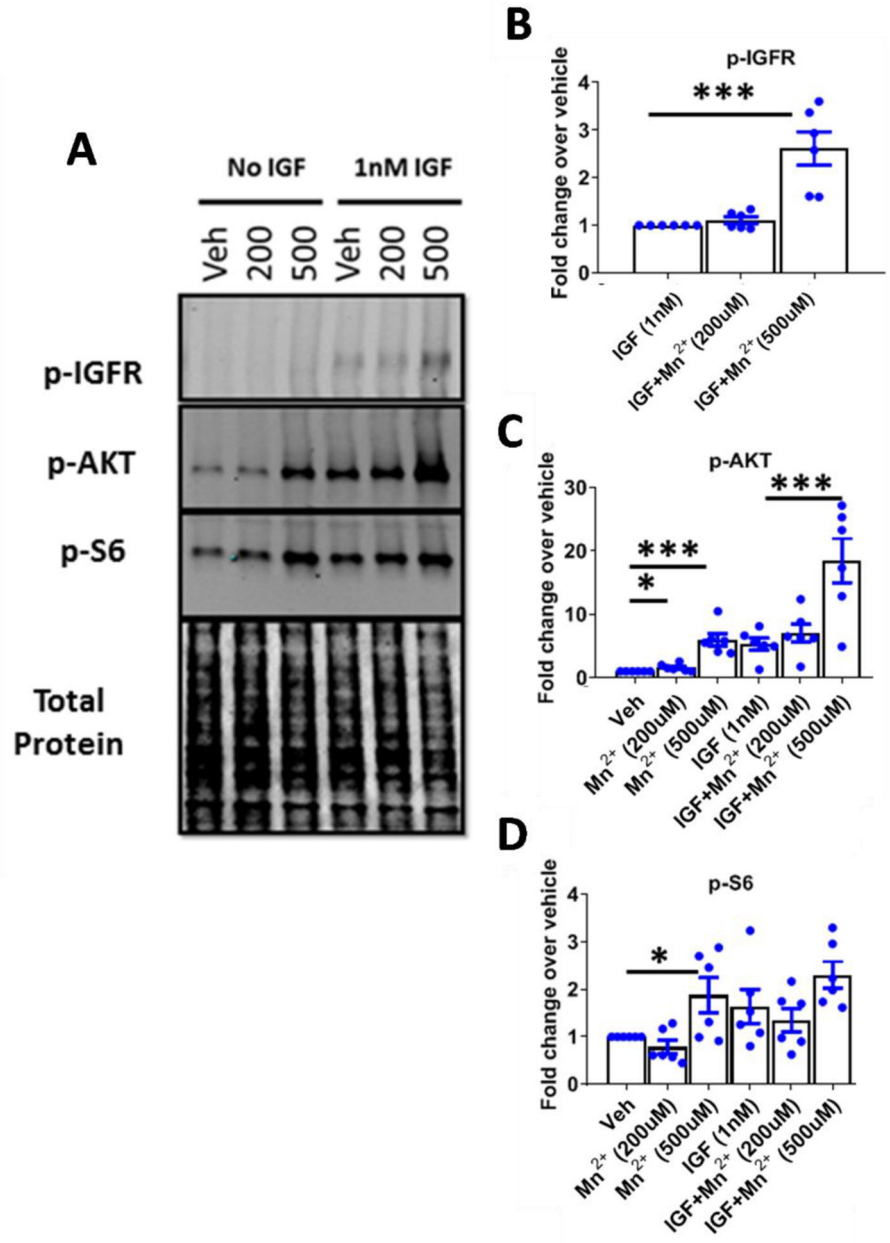

Figure 9: Mn^{2+}-induced p-IGFR/AKT is due to intracellular, not extracellular Mn^{2+}.

A) Representative western blot of control hiPSC-derived neuroprogenitors for p-IGFR, p-AKT, and p-S6 following 3hr Mn^{2+} exposure with 200/500μM Mn^{2+} in HBSS, 3X HBSS washes, then exposure with 1nM IGF (without Mn^{2+}) or HBSS (no IGF or Mn^{2+}) for another 3hrs. **B-D**) Quantifications of p-IGFR **(B)** One-way ANOVA for treatment $F(2,6)= 116.5$; $p<.0001$, p-AKT **(C)** One-way ANOVA for treatment $F(5,15)= 107.2$; $p<.0001$, and p-S6 (**D**) One-way ANOVA for treatment $F(5,15)= 14.12$; $p<.0001$. N=6 (two differentiations of three separate control patients); Error bars= SEM. *= significance by Tukey multiple comparison test. *P<.05, **P<.01, ***P<.001.

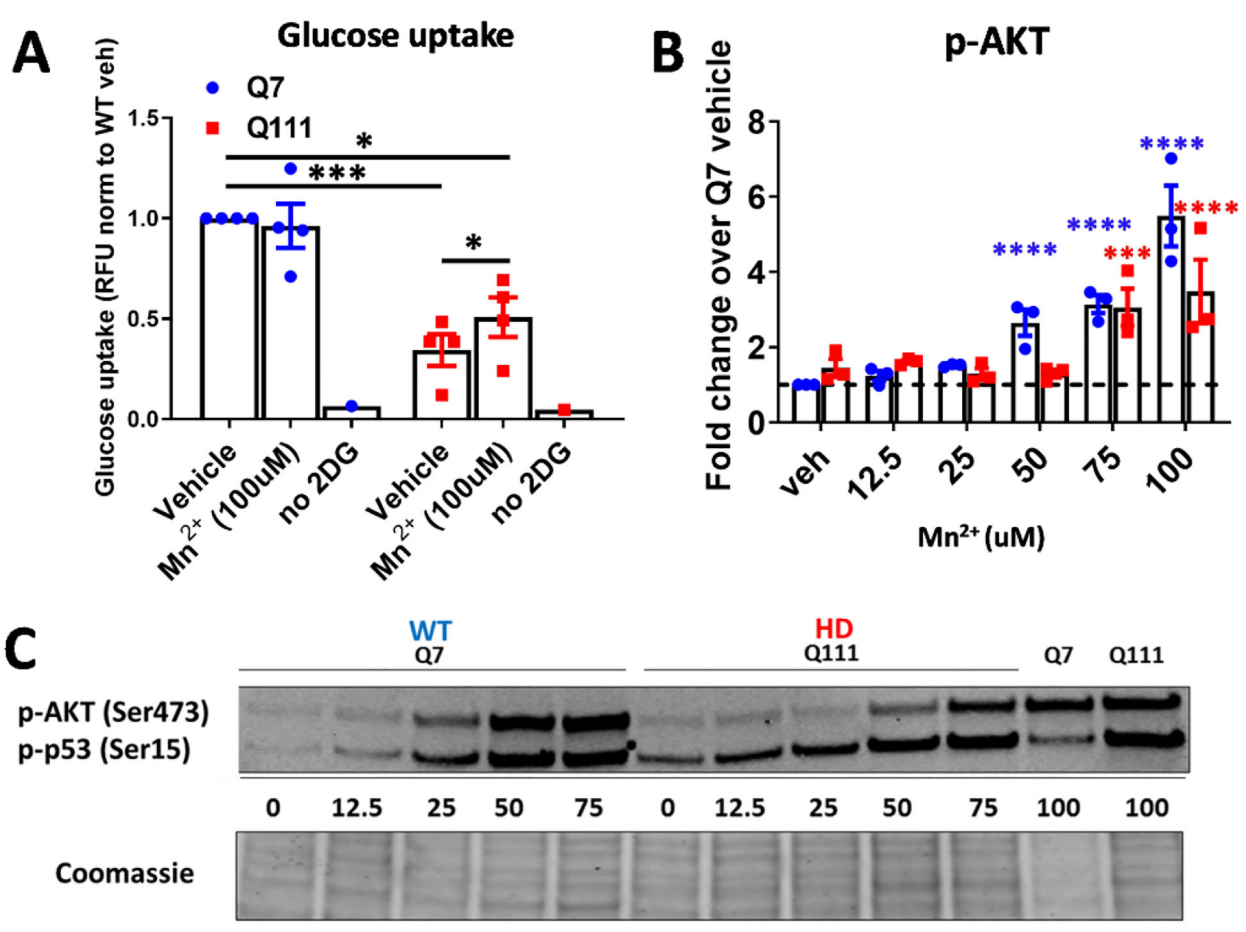

Figure 10: Mn^{2+} increases glucose uptake in Q111 cells.

A) Quantification of glucose uptake in STHdh Q7/Q7 and Q111/Q111 following 24hr exposure with 50/100μM Mn^{2+}. "no 2DG" is a negative control in which no glucose was added to cells. N=4; Error bars= SEM. Two-way ANOVA; treatment= F(2,6)=1.443 p=<0.3079; genotype= F(1,3)= 5.585 p=0.0991; treatment-genotype interaction= F(2,6)= 5.939 p=.0370. *= significance by Tukey's multiple comparison test. **B)** Quantification of p-AKT (p-p53 is not quantified) across 12.5–100uM Mn exposure. Two-way ANOVA; treatment= F(5,10)=29.75; p=<0.0001; genotype= F(1,2)=35.45; p=0.0271. *= significant by Sidak's multiple comparison. *P<.05, **P<.01, ***P<.001. **C)** Representative western blot of p-AKT and p-p53 after 24hr Mn exposure with 12.5–100uM in WT and HD STHdh cells